Cell Reports

Article

Antigenic sin and multiple breakthrough infections drive converging evolution of COVID-19 neutralizing responses

Graphical abstract

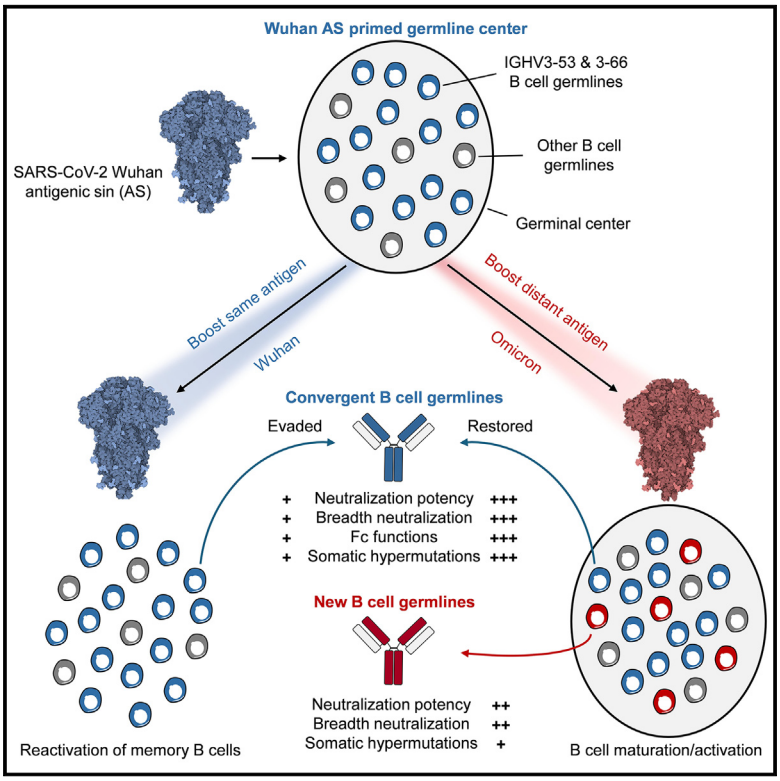

Highlights

- Omicron infection induces potent neutralization and Fc functions against variants
- Neutralization relies on restored germ lines expanded by Wuhan antigenic sin (AS)
- AS drives convergent antibody maturation in homologous and heterologous immunity
- Omicron infection stretches the antibody repertoire to control SARS-CoV-2 variants

Authors

Ida Paciello, Giulio Pierleoni, Elisa Pantano, ..., Olivier Schwartz, Rino Rappuoli, Emanuele Andreano

Correspondence

e.andreano@toscanalifesciences.org

In brief

Paciello et al. find that Omicron infection induces the most potent and broad antibody response to SARS-CoV-2 variants. This response relies on restored B cell germ lines expanded by the Wuhan antigenic sin, like IGHV3-53 and 3-66, and on new germ lines expanded to stretch the antibody repertoire to control SARS-CoV-2 variants.

Paciello et al., 2024, Cell Reports *43*, 114645
September 24, 2024
https://doi.org/10.1016/j.celrep.2024.114645

CellPress

Cell Reports

CellPress
OPEN ACCESS

Article

Antigenic sin and multiple breakthrough infections drive converging evolution of COVID-19 neutralizing responses

Ida Paciello,[1] Giulio Pierleoni,[1,2] Elisa Pantano,[1,2] Giada Antonelli,[1] Piero Pileri,[1] Giuseppe Maccari,[3] Dario Cardamone,[3] Giulia Realini,[1] Federica Perrone,[1,2] Martin Mayora Neto,[4] Simone Pozzessere,[5] Massimiliano Fabbiani,[6,7] Francesca Panza,[6] Ilaria Rancan,[6] Mario Tumbarello,[6,7] Francesca Montagnani,[6,7] Duccio Medini,[3] Piet Maes,[8] Nigel Temperton,[4] Etienne Simon-Loriere,[9,10] Olivier Schwartz,[11,12] Rino Rappuoli,[2,14] and Emanuele Andreano[1,15,*]

[1]Monoclonal Antibody Discovery (MAD) Lab, Fondazione Toscana Life Sciences, Siena, Italy
[2]Department of Biotechnology, Chemistry, and Pharmacy, University of Siena, Siena, Italy
[3]Data Science for Health (DaScH) Lab, Fondazione Toscana Life Sciences, Siena, Italy
[4]Viral Pseudotype Unit, Medway School of Pharmacy, Universities of Kent and Greenwich, Chatham Maritime, Kent, UK
[5]Department of Cellular Therapies, Hematology, and Laboratory Medicine, University Hospital of Siena, Siena, Italy
[6]Department of Medical Sciences, Infectious and Tropical Diseases Unit, Siena University Hospital, Siena, Italy
[7]Department of Medical Biotechnologies, University of Siena, Siena, Italy
[8]KU Leuven, Rega Institute, Department of Microbiology, Immunology, and Transplantation, Laboratory of Clinical and Epidemiological Virology, Leuven, Belgium
[9]G5 Evolutionary Genomics of RNA Viruses, Institut Pasteur, Université Paris Cité, Paris, France
[10]National Reference Center for Respiratory Viruses, Institut Pasteur, Paris, France
[11]Virus and Immunity Unit, Department of Virology, Institut Pasteur, Paris, France
[12]Vaccine Research Institute, Creteil, France
[14]Fondazione Biotecnopolo di Siena, Siena, Italy
[15]Lead contact
*Correspondence: e.andreano@toscanalifesciences.org
https://doi.org/10.1016/j.celrep.2024.114645

SUMMARY

Understanding the evolution of the B cell response to severe acute respiratory syndrome coronavirus 2 (SARS-CoV-2) variants is fundamental to design the next generation of vaccines and therapeutics. We longitudinally analyze at the single-cell level almost 900 neutralizing human monoclonal antibodies (nAbs) isolated from vaccinated people and from individuals with hybrid and super hybrid immunity (SH), developed after three mRNA vaccine doses and two breakthrough infections. The most potent neutralization and Fc functions against highly mutated variants belong to the SH cohort. Repertoire analysis shows that the original Wuhan antigenic sin drives the convergent expansion of the same B cell germlines in vaccinated and SH cohorts. Only Omicron breakthrough infections expand previously unseen germ lines and generate broadly nAbs by restoring IGHV3-53/3-66 germ lines. Our analyses find that B cells initially expanded by the original antigenic sin continue to play a fundamental role in the evolution of the immune response toward an evolving virus.

INTRODUCTION

The severe acute respiratory syndrome coronavirus 2 (SARS-CoV-2) has shown an incredible ability to evolve and evade immunity induced by infection and vaccination as well as monoclonal antibodies (mAbs) for treatment and prevention of COVID-19. Since the beginning of the COVID-19 pandemic, over 70 major variants have emerged, highlighting the plasticity of this virus and its ability to adapt to the human immune response over time.[1] The initial antibody response induced by SARS-CoV-2 infection was dominated by immunoglobulin heavy variable (IGHV)3-53/3-66-encoded antibodies, which were able to potently neutralize the original Wuhan virus, in their germline-like state.[2–8] These antibodies target the Spike (S) protein receptor binding domain (RBD), which is overall the main target for SARS-CoV-2 neutralizing antibodies (nAbs).[8–10] Given the high immune pressure generated by these germ lines, the virus rapidly introduced the N501Y, E484K, and K417N mutations, which evaded almost 60% of antibodies encoded by IGHV3-53/3-66 germ lines induced by infection or mRNA vaccination.[2,7] The subsequent waves of the pandemic were driven by SARS-CoV-2 variants with an increased number of mutations in the S protein. Specifically, the appearance of the first Omicron variants (BA.1 and BA.2) at the end of 2021 marked a new chapter in the COVID-19 pandemic.[11,12] The BA.1 and BA.2 variants harbored 37 and 31 mutations in the S protein that showed unprecedented immune evasion levels, reducing drastically the neutralizing efficacy of sera from infected and vaccinated people and evading almost 90% of IGHV3-53/3-66

gene-derived nAbs.[13–16] From 2022 onward, several Omicron variants appeared worldwide with an increased number of mutations and immune evasion levels, starting from BA.5 to BA.2.86, the most mutated variant ever observed, carrying almost 60 mutations in the S protein.[17–24] These variants kept spreading and infecting people worldwide, generating a more mature and broadly reactive antibody response to SARS-CoV-2. To understand how the immunological response adapted and matured to SARS-CoV-2 variants over time, we longitudinally analyzed at the single-cell level almost 900 nAbs isolated from 4 different cohorts: seronegative donors that received 2 mRNA vaccine doses (SN2); the same donors in SN2 subsequently re-enrolled when they received a third booster dose (SN3); seropositive subjects with hybrid immunity (i.e., 1 infection and 2 mRNA vaccine doses [SP2]); and seropositive donors with super hybrid immunity (SH) (i.e., at least 3 mRNA vaccine doses and 2 breakthrough infections). Part of the donors in this cohort were re-enrolled from the SP2 group. The direct comparison of our four different cohorts revealed that SH had the strongest antibody response against all tested variants. In addition, while the initial Omicron cross-neutralizing response induced by vaccination or infection was mediated by different germ lines,[25] after Omicron breakthrough infection, the original Wuhan antigenic sin drove a convergent expansion of the same B cell germ lines in vaccinated and SH cohorts. Indeed, the cross-nAb response in SH was dominated by highly mutated IGHV3-53/3-66 gene-derived nAbs that, after additional infection and vaccination, restored their neutralization and Fc function activities against all variants, including the highly mutated BA.2.86. It is worth noting that SH also expanded previously unseen germ lines to broaden the antibody repertoire with additional B cell germ lines that could be rapidly deployed with the emergence of future SARS-CoV-2 variants. Taken together, our longitudinal single-cell analysis dissects the functional antibody response that has developed in most people and identifies the immunological and genetic features behind cross-protection to highly mutated SARS-CoV-2 variants that could be used to design the next generation of vaccines and therapeutics, and to inform policy makers.

RESULTS

Frequency of B cells and nAbs in SH immunity

In this study, we evaluated the B cell maturation and nAb response of donors with SH —in other words, at least three mRNA vaccine doses and two breakthrough infections. Six donors were analyzed in this work, two of which (VAC-004 and VAC-009) were re-enrolled from our previous study where we evaluated their B cell and antibody response following two mRNA vaccine doses and one breakthrough infection (hybrid immunity).[7] Blood collection for SH donors occurred at an average of 99 days after the last vaccination dose or SARS-CoV-2 breakthrough infection. SH subject details are summarized in Table S1. To evaluate the breadth of reactivity of $CD19^+CD27^+IgD^-IgM^-$ class-switched memory B cell (MBCs) toward different betacoronaviruses, we stained the cells with the S protein of both SARS-CoV-1 and SARS-CoV-2 Wuhan and analyzed the frequencies of single- and double-positive cells (Figure S1A). We selected the SARS-CoV-2 Wuhan S protein as staining bait as all donors were exposed to this antigen. As expected, SH donors showed the highest frequency toward the S protein of SARS-CoV-2, with an average of 0.37% of positive cells, followed by B cells reactive to the SARS-CoV-1 S protein (0.13%) (Table S2). Double-positive MBCs showed the lowest frequency, averaging 0.03% of reactive cells. To evaluate at single level the nAb response of SH donors, SARS-CoV-1 and SARS-CoV-2 Wuhan S protein single- and double-positive MBCs were single cell sorted and incubated for 2 weeks to naturally release human mAbs into the supernatant. A total of 4,505 S $protein^+$ MBCs were sorted and directly tested in neutralization against the live SARS-CoV-2 Wuhan virus and SARS-CoV-1 pseudovirus. Overall, 6.2%–16.3% of antibodies from the 6 SH donors showed the capacity to neutralize at least one virus, resulting in a panel of 545 (12.1%) nAbs (Figure S1B, bottom; Table S2). The initial evaluation of neutralization activity was a qualitative screening where only absence or presence of cytopathic effect was considered as readout of neutralization or not neutralization, respectively. The fraction of nAbs is comparable to what was previously observed for the SN3 (14.4%) and SP2 (14.8%) cohorts.[7,26] Of these, 507 (93.0%), 27 (5.0%), and 11 (2.0%) were able to neutralize live SARS-CoV-2 Wuhan virus, SARS-CoV-1 pseudovirus, or both betacoronaviruses, respectively (Figure S1B, top; Table S2).

Antibody neutralization to SARS-CoV-2 Omicron variants

To better characterize identified nAbs, we tried to express all 545 as immunoglobulin G1 (IgG1) and recovered 419 of them. Of these, 410 (97.8%) neutralized SARS-CoV-2 Wuhan, 7 (1.7%) were cross-neutralizing, and 2 (0.5%) neutralized only SARS-CoV-1. To evaluate their potency and breadth to SARS-CoV-2 and its variants, 417 nAbs (SARS-CoV-2 only and cross-neutralizing) isolated from SH individuals were tested by cytopathic effect-based microneutralization assay against SARS-CoV-2 Wuhan and Omicron BA.5, BA.2.75, BF.7, BQ.1.1, XBB.1.5, EG.5.1.1, and BA.2.86 variants. The data obtained from SH donors were compared with donors seronegative to SARS-CoV-2 infection but vaccinated with 2 (SN2; n = 5) or 3 (SN3; n = 4) mRNA vaccine doses, and with seropositive subjects with hybrid immunity (2 mRNA vaccine doses and 1 breakthrough infection; SP2; n = 5) (Figures 1A–1D, S1C, S1D, and S2A–S2D). From SN2, SN3, and SP2, we previously isolated 52, 206, and 224 nAbs, respectively.[7,26] Neutralization potency was expressed as 100% inhibitory concentration (IC_{100}) and the evaluation of all antibodies in each cohort as geometric mean IC_{100} ($GM\text{-}IC_{100}$). SH donors had an overall higher percentage of nAbs neutralizing all SARS-CoV-2 Omicron variants (Figures 1A–1D; Table S3). Only one nAb (1.9%) was able to neutralize BF.7 and BQ.1.1 in the SN2 while none of the antibodies in this cohort showed neutralization activity against the other Omicron variants tested (Figures 1A and S2A). In contrast, higher levels of cross-protection were observed in SN3, SP2, and SH. The frequencies of nAbs from SN3 donors neutralizing Omicron BA.5, BA.2.75, BF.7, BQ.1.1, XBB.1.5, EG.5.1.1, and BA.2.86 variants were 12.1 (n = 23), 17.0 (n = 32), 10.2 (n = 21), 5.8 (n = 15), 7.3 (n = 14), 3.4 (n = 7), and 2.9% (n = 6), while these variants were neutralized by 13.4 (n = 30), 3.6 (n = 8), 9.8 (n = 22), and 5.8% (n = 13) of

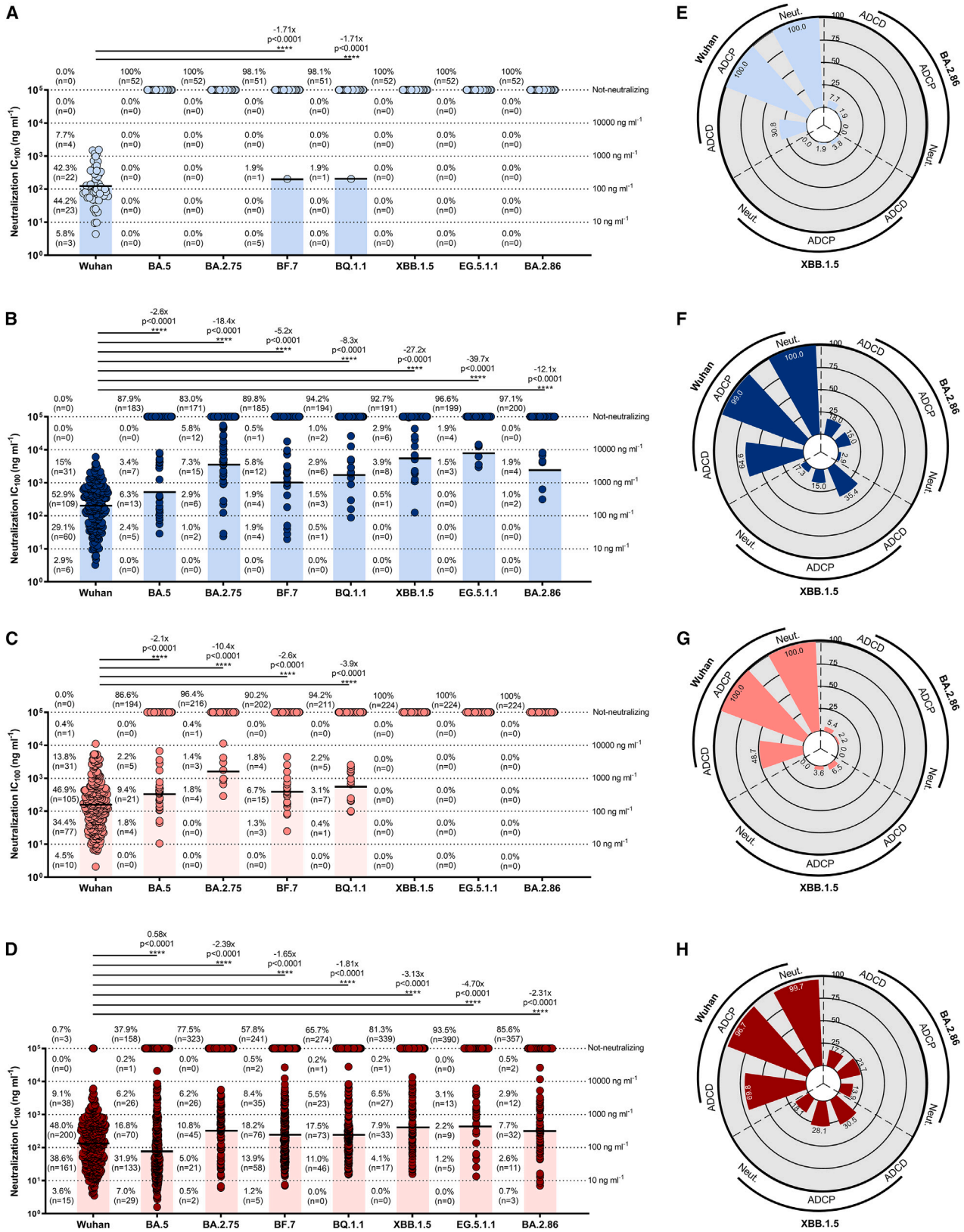

(legend on next page)

SP2 antibodies (Figures 1B, 1C, S2B, and S2C). None of the nAbs in the SP2 cohort were able to neutralize XBB.1.5, EG.5.1.1, and BA.2.86 variants. Finally, the frequencies of nAbs from SH donors neutralizing BA.5, BA.2.75, BF.7, BQ.1.1, XBB.1.5, EG.5.1.1, and BA.2.86 variants were 62.1 (n = 259), 22.5 (n = 94), 42.2 (n = 175), 34.3 (n = 143), 18.7 (n = 76), 6.5 (n = 27), and 14.4% (n = 60), respectively (Figures 1D and S2D). The four cohorts showed similar neutralization potencies against SARS-CoV-2 Wuhan, nAbs isolated from SH donors had the highest neutralization potencies against all Omicron variants tested, and it was the only cohort with nAbs showing a potency below 10 ng mL^{-1} (Figures 1A–1D, S1C, and S1D; Tables S3 and S4). To understand the S protein domains targeted by antibodies isolated from SH donors, nAbs were tested for binding against the RBD, N-terminal domain (NTD), and the S2 domain of the original Wuhan SARS-CoV-2 S protein. In all SH subjects, nAbs targeted mainly the RBD (n = 317; 75.3%), followed by NTD (n = 81; 19.2%) and S protein (n = 23; 5.5%) (Figure S2E; Table S4). No S2 domain-binding nAbs were identified. This distribution is in line with what was previously observed in donors with three mRNA vaccine doses and with hybrid immunity.[26]

Evaluation of Fc effector functions to XBB.1.5 and BA.2.86

Next, we evaluated the antibody-dependent phagocytic activity (ADCP) and antibody-dependent complement deposition (ADCD) of all identified nAbs in SH against the ancestral Wuhan virus, the XBB.1.5 variant that dominated from February to May 2023, and the highly mutated SARS-CoV-2 variant BA.2.86, ancestral germ line of the currently predominant JN.1 variant (Figures 1E–1H). The Fc functions were evaluated for nAbs that retained the binding to the XBB.1.5 and BA.2.86 S proteins (Figure S3A). Binding nAbs were 7.7 (n = 4), 43.7 (n = 90), 11.6 (n = 26), and 39.8% (n = 166) for XBB.1.5 and 7.7 (n = 4), 18.0 (n = 37), 5.8 (n = 13), and 27.6% (n = 115) for BA.2.86 in SN2, SN3, SP2, and SH, respectively. While no neutralization was observed against XBB.1.5 and BA.2.86, a low fraction of nAbs retained ADCP and ADCD activities in the SN2 (1.9%–7.8%) and SP2 (2.2%–6.5%) cohorts (Figures 1E and 1G). Differently, a bigger fraction of nAbs in SN3 and SH retained both neutralization and Fc functions. Indeed, 15.0%–35.4% of nAbs in the SN3 cohort were able to induce ADCP and ADCD against XBB.1.5 and BA.2.86, while 17.7–30.5% of antibodies retained these activities in the SH cohort (Figures 1F and 1H). Next, we evaluated the Fc function potencies induced by nAbs in the four different cohorts and the S protein domains mainly involved in these activities (Figures S3B–S3E). No major differences were observed in the SN2 cohort for S protein trimer, RBD, and NTD-binding nAbs (Figure S3B). However, the low number of antibodies active against XBB.1.5 and BA.2.86 made this evaluation difficult. Differently, a third booster dose (SN3) or hybrid immunity (SP2) improved nAb Fc activities, despite losing potency against tested variants. In the SN3 cohort, NTD-binding nAbs showed the strongest ADCD activity while similar levels of activity are observed for ADCP (Figure S3C). In SP2, RBD- and NTD-binding nAbs showed similar potency, which is higher than what was observed for S protein trimer-targeting antibodies (Figure S3D). As for the SH cohort, nAbs binding the NTD showed the strongest ADCP and ADCD activities (Figure S3E). A possible explanation as for why NTD-targeting nAbs induce higher Fc functions is that these antibodies, while binding to their epitope, present a geometry and stoichiometry of the Fc portion that facilitates and increases the availability to FcRs, resulting in higher effector functions. Overall, our analyses of the Fc functions showed that antibodies lacking neutralization can still retain Fc functions that support the immune response to SARS-CoV-2 variants. This observation could explain the lower severity of infection following infection with recent SARS-CoV-2 variants.[27]

Antibody potency and breadth to alpha and beta human coronaviruses

To assess the breadth of neutralization to other alpha and beta human coronaviruses (h-CoV), in addition to SARS-CoV-1 and -2, we tested all nAbs isolated in the SH cohort against HKU-1, 229E, and OC43. Initially, we evaluated the binding activity of all nAbs to the h-CoV S proteins. Our data showed that over 94.0% of nAbs were specific for SARS-CoV-2 only. Only, 3.8 (n = 20), 1.0 (n = 7), 0.3 (n = 2), and 0.1% (n = 1) of SARS-CoV-2 nAbs showed binding to SARS-CoV-1, OC43, 229E, and HKU-1 respectively (Figure 2A; Table S4). We next evaluated the neutralization activity and potency of cross-binding nAbs to SARS-CoV-1, OC43, 229E, and HKU-1 pseudoviruses. Neutralization potency for pseudoviruses was expressed as 50% neutralization dose (ND_{50}) and the evaluation of all antibodies in each cohort as geometric mean ND_{50}. Our results revealed that 45.0% (n = 9) of SARS-CoV-1 S protein-binding nAbs were neutralizing, with an ND_{50} ranging from 54.2 to 22,000.4 ng mL^{-1}. Similarly, 57.1% (n = 4) of nAbs reacting to OC43 S protein also showed neutralization activity but with an overall low potency, with an ND_{50} ranging from 804.0 to 38,490.0 ng mL^{-1}. The single nAb reacting to HKU-1 poorly neutralized the pseudovirus (ND_{50} 29,030.0 ng mL^{-1}), while the two 299E S protein-binding nAbs did not show neutralization activity against this alpha coronavirus (Figure 2B).

Epitope mapping of cross-neutralizing nAbs

To understand the S protein regions mainly involved in cross-protection against the Omicron variants, we investigated the

Figure 1. nAbs potency and breadth of neutralization and Fc functions against SARS-CoV-2 Omicron variants

(A–D) Scatter dot charts show the neutralization potency, reported as IC_{100} (ng mL^{-1}), of nAbs tested against the original Wuhan SARS-CoV-2 virus and the Omicron BA.5, BA.2.75, BF.7, BQ.1.1, XBB.1.5, EG.5.1.1, and BA.2.86 lineages for SN2 (A), SN3 (B), SP2 (C), and SH (D). The number, percentage, GM-IC_{100} (black lines and colored bars), fold change, and statistical significance of nAbs are denoted on each graph. Reported fold change and statistical significance are in comparison with the Wuhan virus. Technical duplicates were performed for each experiment.

(E–H) Doughnut charts show the frequency of nAbs retaining neutralization (Neut.), ADCP and ADCD against the SARS-CoV-2 Wuhan virus, and the XBB.1.5 and BA.2.86 variants for SN2 (E), SN3 (F), SP2 (G), and SH (H). A nonparametric Mann-Whitney t test was used to evaluate statistical significances between groups. Two-tailed p value significances are shown as $^{*}p < 0.05$, $^{**}p < 0.01$, and $^{***}p < 0.001$.

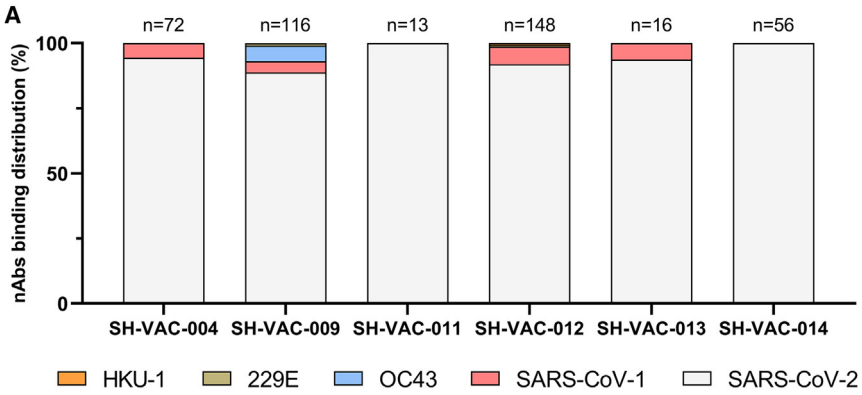

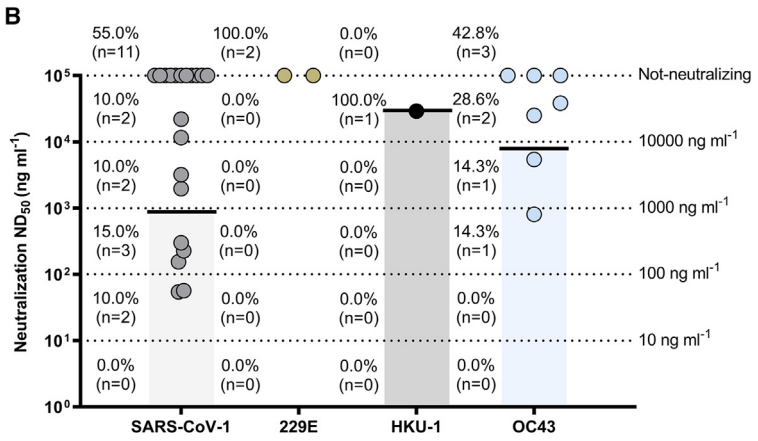

Figure 2. Binding and neutralization activity to alpha and beta h-CoV

(A) The bar graph shows the percentage of nAbs binding to SARS-CoV-2 (light gray), SARS-CoV-1 (pink), OC43 (light blue), 229E (light brown), and HKU-1 (orange) for all donors tested in the SH cohort.

(B) Scatter dot charts show the neutralization potency, reported as ND_{50} (ng mL^{-1}), of nAbs tested against SARS-CoV-1, 229E, HKU-1, and OC43. The number, percentage, and GM-ND_{50} (black lines and colored bars) are denoted on each graph. Technical duplicates were performed for each experiment.

neutralization activity of RBD- and NTD-targeting nAbs (Figure 3). RBD-targeting nAbs were classified based on their ability to compete with the class 1/2 antibody J08,[28] the class 3 antibody S309,[29] and the class 4 antibody CR3022,[30] or for their lack of competition with the three tested antibodies (non-competing).[13,26] The neutralization activity against SARS-CoV-2 Wuhan virus in all cohorts was revealed to be mainly directed to the RBD class 1/2 epitope region (Figures 3A–3D). In the SN2 group ($n = 46$), we observed a lack of neutralization activity against most Omicron variants tested, except for one NTD-targeting nAb that neutralized both BF.7 and BQ.1.1 (Figure 3A). In the SN3 cohort ($n = 197$), after a third booster dose, we observed a more cross-reactive antibody response, with 3.0%–16.8% of nAbs able to neutralize all Omicron variants tested. The majority of these nAbs were directed against the RBD class 1/2 epitope region (Figure 3B). The SP2 cohort ($n = 215$) showed 3.7%–14.0% of cross-protection against Omicron BA.5, BA.2.75, BF.7, and BQ.1.1, while no neutralization was observed to XBB.1.5, EG.5.1.1, and BA.2.86. In this cohort, cross-neutralization was mainly driven by NTD and RBD class 3 targeting nAbs (Figure 3C). After a subsequent infection and additional vaccine dose, the antibody response in the SH cohort ($n = 413$) showed a different profile. Cross-neutralization was observed against all tested Omicron variants, with a frequency ranging from 6.5% to 62.7%. Of note, the majority of cross-neutralizing nAbs in the SH cohort were directed toward the RBD class 1/2 region, changing the target profile compared to the less mature SP2 immune response (Figure 3D). When we evaluated the neutralization potency, expressed as IC_{100}, of cross-neutralizing nAbs, we observed in all cohorts that RBD-binding antibodies were more potent than the NTD-targeting group (Figures S4A–S4G; Table S5). As for the different RBD classes, our data showed that class 3 nAbs were overall the most potent against Omicron variants in the SP2 cohort, showing up to 2.6- and 8.7-fold lower GM-IC_{100} compared to class 1/2 and 4 nAbs, respectively. In contrast, the most potent nAbs in the SN3 and SH cohorts were directed against the class 1/2 epitope region. Overall, class 1/2 nAbs in SN3 were up to 28.9-fold more potent than class 3 antibodies, while in SH, class 1/2 nAbs had a GM-IC_{100} 4.7- and 13.0-fold lower compared to class 3 and 4 antibodies, respectively (Figures S4A–S4G; Table S5). We also evaluated the ADCP and ADCD of all RBD classes and NTD-binding nAbs against XBB.1.5 and BA.2.86. A very small fraction of nAbs in the SN2 cohort, despite not presenting neutralization activity, retained ADCD function (Figure 3E, left). Nevertheless, the low number of nAbs makes it difficult to properly evaluate the Fc response in this cohort. Class 1/2 and NTD-binding nAbs were the most active in the SN3 cohort (Figure 3E, center left). Differently, class 4 nAbs were the most active in the SP2 cohort, and Fc functions were further matured in SH individuals, where up to 85.7% and 57.1% of antibodies belonging to this class showed ADCP and ADCD function, respectively (Figure 3E, center right and right). Further maturation of class 1/2 and 3 in the SH cohort rescued the antibody Fc functions, expanding the fraction of nAbs able to induce ADCP and ADCD compared to SP2 (Figure 3E, center right and right). Our data also highlight the impact of the mutations present on the XBB.1.5 and BA.2.86 S proteins on antibody neutralization and Fc functions. Indeed, the unique set of mutations on the BA.2.86 S protein positioned in the class 3 epitope region (N450D and K356T) seem to be extremely evasive in the SN3 cohort, leading to higher reduction of neutralization, ADCP and ADCD compared to XBB.1.5. Finally, nAbs in the SH cohort

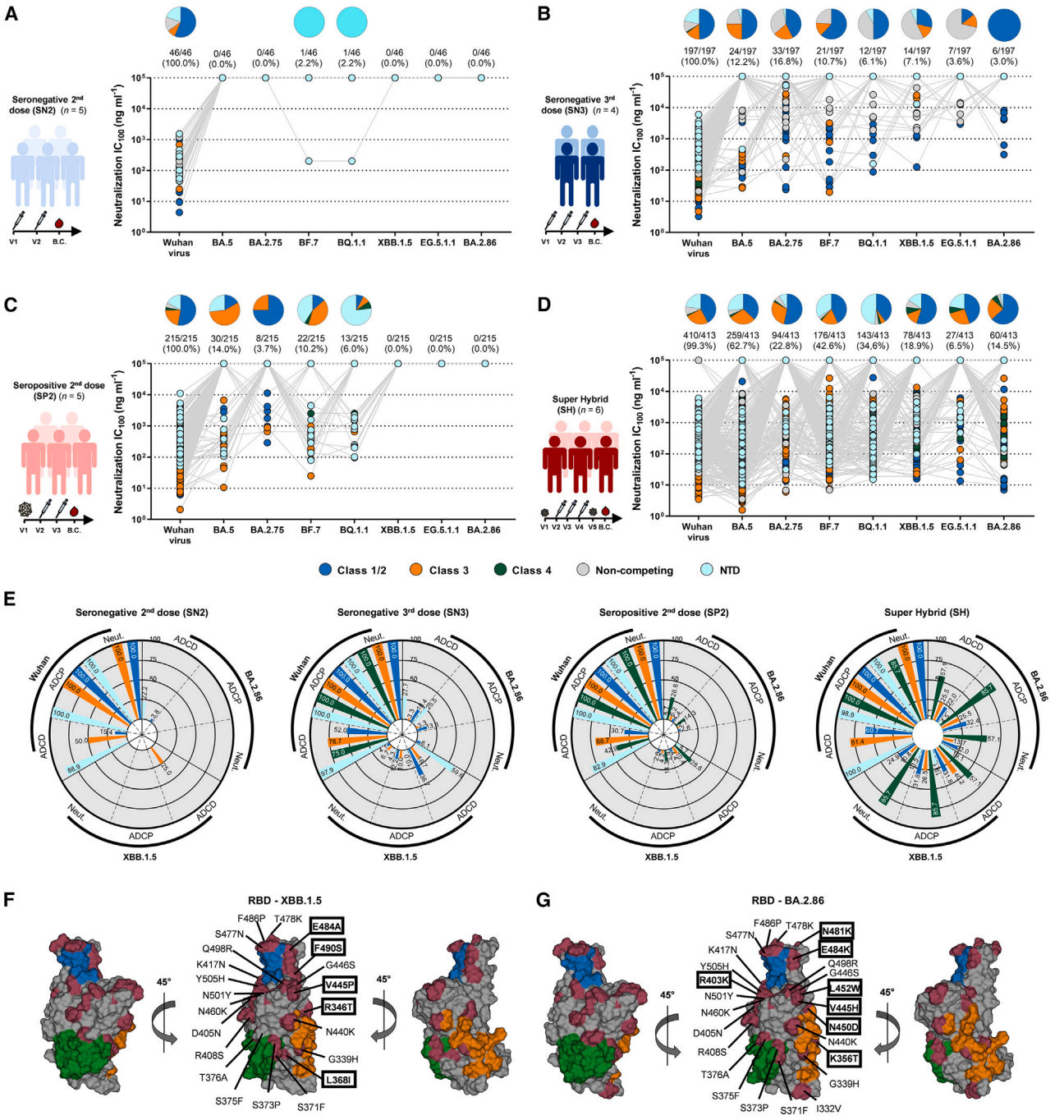

Figure 3. Distribution of RBD and NTD-targeting nAbs against Omicron variants

(A–D) Pie charts show the distribution of cross-neutralizing nAbs based on their ability to target class 1/2 (blue), class 3 (orange), and class 4 (dark green) regions on the RBD, as well as non-competing nAbs (gray) and NTD-targeting nAbs (cyan). Dot charts show the neutralization potency, reported as IC_{100} (ng mL^{-1}), of nAbs against the Wuhan virus and the Omicron BA.5, BA.2.75, BF.7, BQ.1.1, XBB.1.5, EG.5.1.1, and BA.2.86 variants observed in the SN2 (A), SN3 (B), SP2 (C), and SH (D) cohorts. The number and percentage of nAbs are denoted on each graph.

(E) Radar plots show the frequency of nAbs retaining neutralization, ADCP, and ADCD activities against SARS-CoV-2 Wuhan, XBB.1.5, and BA.2.86.

(F and G) Representation of the SARS-CoV-2 RBD of XBB.1.5 (F) and BA.2.86 (G). In dark red are highlighted the mutations present on the RBD for both variants. Boxed mutated residue labels indicate unique mutations for the specific variant. Class 1/2, 3, and 4 epitope regions are highlighted in blue, orange, and green, respectively.

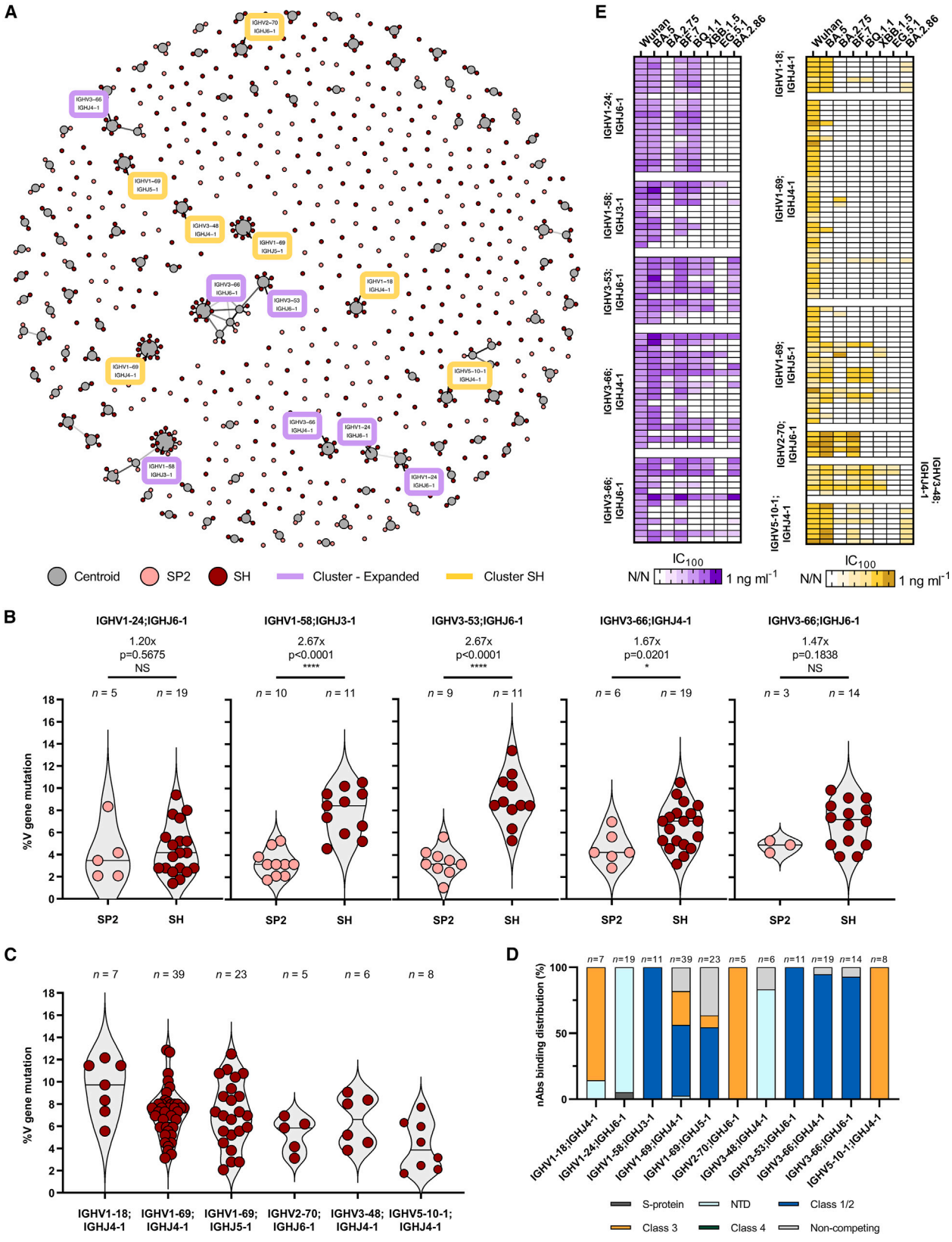

(legend on next page)

showed similar levels of neutralization and Fc functions against both XBB.1.5 and BA.2.86 (Figures 3E–3G).

B cell maturation and expansion in SH immunity

In addition to the neutralization, Fc functions, and epitope mapping analyses, we investigated the B cell expansion and maturation from hybrid (SP2 *n* sequences = 278[7]) to SH immunity (SH *n* sequences = 441). Sequences were clustered by binning the clones to their inferred germ lines (centroids) and according to 80% nucleotide sequence identity in the heavy complementary determining region 3 (CDRH3). Clusters were defined as antibody families including at least five or more members as previously described.[26,31] We found five IGHV and immunoglobulin heavy joining (IGHJ) rearrangements—IGHV1-24;IGHJ6-1, IGHV1-58;IGHJ3-1, IGHV3-53;IGHJ6-1, IGHV3-66;IGHJ4-1, and IGHV3-66;IGHJ6-1—to be predominantly expanded after an additional infection and vaccination dose. In addition, we observed six germ lines—IGHV1-18;IGHJ4-1, IGHV1-69;IGHJ4-1, IGHV1-69;IGHJ5-1, IGHV2-70;IGHJ6-1, IGHV3-48;IGHJ4-1, and IGHV5-10-1;IGHJ4-1—that emerged and expanded only in SH individuals broadening the B cell repertoire in this cohort (Figure 4A). The five germ lines expanded in SH showed 1.20- to 2.67-fold higher somatic hypermutation (SHM) levels compared to SP2, with the IGHV1-58;IGHJ3-1 and IGHV3-53;IGHJ6-1 being the most mutated, with a median V gene mutation of almost 9.0% (Figure 4B). As for the six germ lines found only in SH, we found B cells using the IGHV1-18;IGHJ4-1 rearrangement to be the most mutated, with median V gene mutations of 9.7%, while the IGHV5-10-1; IGHJ4-1 germ line was the least mutated, with a median mutation frequency of 3.9% (Figure 4C). Next, we analyzed the binding and neutralization profiles of germ lines expanded from SP2 or found only SH. The expanded germ lines were found to mainly target the S protein RBD class 1/2 epitope region, with the exception of IGHV1-24;IGHJ6-1, which were found to preferentially bind the NTD (Figure 4D). The neutralization data revealed that IGHV3-53;IGHJ6-1, IGHV3-66;IGHJ4-1, and IGHV3-66;IGHJ6-1 were the most cross-neutralizing germ lines against the SARS-CoV-2 variants tested, with IGHV3-53;IGHJ6-1 showing the highest potency with a GM-IC_{100} of 136.8 ng mL^{-1} (Figure 4E, left; Table S6). The germ lines expanded only in SH were also shown to be mainly directed against the S protein RBD but targeted different regions of the RBD. Indeed, IGHV1-69;IGHJ4-1 and IGHV1-69;IGHJ5-1 targeted mainly the class 1/2, while the germ lines IGHV1-18;IGHJ4-1, IGHV2-70;IGHJ6-1, and IGHV5-10-1;IGHJ4-1 were directed almost exclusively toward the class 3 epitope region. Interestingly, the germline IGHV3-48;IGHJ4-1 preferentially recognized the NTD and was shown to be the most cross-neutralizing, covering 7 out of 8 (87.5%) SARS-CoV-2 variants tested in this study, with a GM-IC_{100} of 167.1 ng mL^{-1} (Figure 4E). Conversely, the broadly expanded RBD-targeting germline IGHV1-69;IGHJ4-1 showed the lowest level of cross-protection, despite some nAbs in this group being highly mutated and carrying almost 13% of mutations in the V gene (Figure 4E, right; Table S6).

B cell convergence after homologous or heterologous immunization

Next, we compared the evolution of the B cell repertoire in the SN3 (*n* sequences = 289[26]) and SH cohorts. Interestingly, we observed a strong convergence of the B cell response in these two groups that shared the expansion of five different B cell rearrangements, IGHV1-58; IGHJ3-1, IGHV1-69; IGHJ3-1, IGHV1-69; IGHJ4-1, IGHV3-53; IGHJ6-1 and IGHV3-66; IGHJ6-1 (Figure 5A). The five germ lines, known to encode for potently neutralizing RBD-targeting Class 1 and Class 2 nAbs,[13,30,32,33] constituted 27.0 (*n* = 78) and 22.7% (*n* = 100) of the whole functional B cell repertoire in SN3 and SH respectively (Table S7). While these germ lines were predominantly expanded in both SN3 and SH, they showed different neutralization profiles against SARS-CoV-2 Wuhan and Omicron variants. Indeed, in the SN3 cohort, nAbs derived from IGHV1-69; IGHJ4-1 germ lines were the most cross-reactive even if they showed a low to medium neutralization potency with a GM-IC_{100} of 2,065.1 ng mL^{-1} (Figure 5B, top panel; Table S6). Differently, in the SH cohort, IGHV1-69; IGHJ4-1 derived-nAbs were the least cross-reactive while antibodies encoded by the other four predominant germ lines showed improved neutralization potency and breadth. The IGHV3-53;IGHJ6-1 and IGHV3-66;IGHJ6-1 were found to encode for the most cross-neutralizing nAbs with a GM-IC_{100} of 136.8 and 176.4 ng mL^{-1} respectively, which is 2.99- and 2.84-fold more potent of nAbs encoded by the same germ lines in the SN3 cohort (Figure 5B, bottom; Table S6). These germ lines showed broad neutralization against all variants, including the highly mutated BA.2.86 (14/25; 56.0%), while only 2 out of 25 (8.0%) of these nAbs were able to cover the EG.5.1.1 variant, which was predominant in Europe from July 2023 to November 2023, before the surge of JN.1. We then evaluated the Fc functions induced by the five predominant germ lines against the SARS-CoV-2 Wuhan, XBB.1.5, and BA.2.86 viruses and again observed different functional profiles. Indeed, IGHV1-69;IGHJ4-1 gene-derived nAbs in SN3 showed the strongest ADCP and ADCD compared to antibodies encoded by the same germ lines in the SH cohort (Figure 5C, left), while IGHV3-53;IGHJ6-1 and IGHV3-66;IGHJ6-1 nAbs in SH showed

Figure 4. SH germline expansion and characterization

(A) Network plot shows the clonally expanded antibody families in SP2 and SH. Centroids and nAbs from SP2 and SH groups are shown in gray, pink, and dark red, respectively. Clusters and expanded clones are highlighted in gold and dark red, respectively.

(B and C) The violin plots show the V gene somatic mutation frequency of germ lines expanded from SP2 to SH (B) or found exclusively in SH (C). The number of nAbs for each germ line and fold change are denoted on each graph. Violin plots show the median of V gene mutations. A nonparametric Mann-Whitney t test was used to evaluate statistical significances between groups. Two-tailed *p* value significances are shown as $^{*}p < 0.05$ and $^{***}p < 0.0001$. Not significant *p* values were denoted on the figure as "NS."

(D) Bar graphs show the distribution of nAbs binding the S protein trimer (light gray), NTD (cyan), and RBD (dark gray) for expanded germ lines. The number of nAbs per each germ line is denoted on the graph.

(E) The heatmap shows the IC_{100} of predominant germ lines expanded from SP2 to SH (left) or found exclusively in SH (right).

(legend on next page)

the strongest Fc functions in this cohort (Figure 5C, right; Table S8). When we analyzed the SHM levels of nAbs encoded by the five predominant germ lines, we observed that only IGHV1-69;IGHJ4-1 nAbs had similar levels of V gene mutations between SN3 and SH. The remaining predominant germ lines showed 1.24- to 1.57-fold higher levels of V gene mutations in SH with IGHV1-69;IGHJ3-1 and IGHV3-53;IGHJ6-1 being the most mutated (Figure 6A). In addition to shared germ lines, we observed that SH had unique germ lines not expanded in the SN3 cohort. The five most abundant were the IGHV1-18;IGHJ4-1, IGHV1-2;IGHJ4-1, IGHV1-24;IGHJ4-1, IGHV3-21;IGHJ6-1, and IGHV5-10-1;IGHJ4-1 (Figure 5A). Interestingly, IGHV1-18;IGHJ4-1 and IGHV5-10-1;IGHJ4-1 were not found in the SP2 cohort and were exclusive to the SH group. Antibodies from the IGHV1-24;IGHJ4-1, IGHV3-21;IGHJ6-1, and IGHV5-10-1;IGHJ4-1 germ lines showed the highest cross-neutralization activity, covering 75% of tested SARS-CoV-2 variants, with a GM-IC_{100} of 289.0, 287.1, and 91.3, respectively (Figure 6B; Table S7). These three germ lines were also the least mutated, with an average V gene mutations frequency below 6.0%, suggesting space for further maturation of these nAbs (Figure 6C).

DISCUSSION

In this study, we used a panel of almost 900 mAbs to compare the SARS-CoV-2 neutralizing response induced by two or three mRNA vaccines doses, by hybrid immunity, and by multiple vaccinations and breakthrough infections. In line with recent studies,[34,35] our data revealed that while the initial antibody response was different in vaccinated or infected people, breakthrough infections by a distantly related virus such as Omicron induced the expansion of previously unseen germ lines and, most important, rescued the B cell primed by the original antigenic sin. In the case of IGHV3-53/3-66, Omicron breakthrough infection induced convergent restoration of the neutralizing activity of these germ lines, generating strong and cross-reactive antibody responses against SARS-CoV-2 variants, including the highly mutated BA.2.86. Interestingly, the antibody response in SH remained focused mainly on SARS-CoV-2, as less than 10% of nAbs showed cross-reactivity to other alpha and beta h-CoV. The most abundant class of nAbs after homologous immunization, independently from two or three mRNA vaccine doses, is the class 1/2. Further maturation of the SP2 antibody response redirects nAbs from class 3 and NTD to class 1/2, converging with the antibody response observed after homologous immunization. Surprisingly, the main B cell germ lines that stood behind the high levels of cross-protection observed in SH were antibodies encoded by the IGHV3-53/3-66 genes, which were highly evaded by all Omicron variants in less mature immunological responses like SN2, SN3, and SP2.[13,14] This observation suggests that the B cell compartment, after additional maturation following repeated immunizations or breakthrough infections, prefers to resiliently restore and expand germ lines induced by the initial SARS-CoV-2 Wuhan S protein (i.e., the antigenic sin) over naive B cells. Therefore, independently from the priming that individuals received after vaccination or infection, we observed a strong convergence in the antibody response. Of note, up to 56% of IGHV3-53/3-66 encoded nAbs were able to neutralize the highly mutated BA.2.86 variant, while only 8% of these nAbs cross-protected against EG.5.1.1. This observation highlights the importance of the highly conserved residue Y33 placed in the heavy-chain complementary determining region 1 of IGHV3-53/3-66-encoded nAbs as it was previously shown to form extensive hydrophobic interactions with the RBD residue F456 mutated exclusively on the EG.5.1.1 lineage (F456L).[17,32] In addition, this observation could explain, at the single-cell level, why the highly mutated BA.2.86 did not become predominant worldwide despite exhibiting substantial antigenic drift, remarkably enhanced receptor binding affinity, fusogenicity, and infectivity to lung cells compared to other variants.[36–38] Anyway, BA.2.86 rapidly evolved, and at the end of 2023, the JN.1 sublineage emerged, becoming the predominant variant worldwide. JN.1 carries only one additional mutation in the RBD, L455S, compared to the ancestral BA.2.86 variant, which resulted in decreased angiotensin-converting enzyme 2 affinity but enhanced immune evasion.[39,40] Future work will help us to understand the classes of antibodies evaded and the germ lines that are still able to retain neutralization against JN.1. Indeed, we identified low mutated B cell germ lines uniquely expanded in SH (IGHV1-18; IGHJ4-1 and IGHV5-10-1; IGHJ4-1), suggesting a stretch of the antibody repertoire that could be rapidly deployed against future SARS-CoV-2 variants, including JN.1. Overall, our work provides unique information on the longitudinal evolution of the B cell compartment in response to SARS-CoV-2 variants, highlighting similarities and differences between homologous and heterologous vaccination, and how the imprinting of the antigenic sin plays a fundamental role by restoring and driving antibody maturation. Recent findings show that the antibody response to Omicron-based boosters in humans is dominantly imprinted by the Wuhan original antigenic sin, which is beneficial to drive the expansion of cross-nAbs against SARS-CoV-2 variants.[34,41] However, multiple Omicron booster doses or breakthrough infections can subvert or mitigate the impact of the Wuhan original antigenic sin, leading to a more variant specific B cell and antibody response.[35,42] The data generated in this work may be useful to inform the design of the next generation of vaccines and therapeutics, and to inform

Figure 5. B cell repertoire and functional characterization of predominant germ lines

(A) Heatmaps and alluvial plots display the antibody IGHV;IGHJ gene rearrangements frequency for each single donor and for pulled nAbs, respectively, for SN3 (left) and SH (right). In the alluvial plots, the top five shared V-J gene rearrangements shared between SN3 and SH were highlighted. Selected germ lines were highlighted in light purple, green, dark green, gold, and brown for IGHV1-58;IGHJ3-1, IGHV1-69;IGHJ3-1, IGHV1-69;IGHJ4-1, IGHV3-53;IGHJ6-1, and IGHV3-66;IGHJ6-1, respectively. Box with black borders in the stratum identify the top five germ lines expanded exclusively in SH.

(B) Heatmaps show the neutralization activity for the five most shared germ lines between SN3 and SH against BA.5, BA.2.75, BF.7, BQ.1.1, XBB.1.5, EG.5.1.1, and BA.2.86.

(C) Radar plots describe the neutralization, ADCP, and ADCD activities of predominant germ lines shared between SN3 and SH against Wuhan, XBB.1.5, and BA.2.86. The percentages of functionality for neutralization, ADCP, and ADCD are reported within each radar plot.

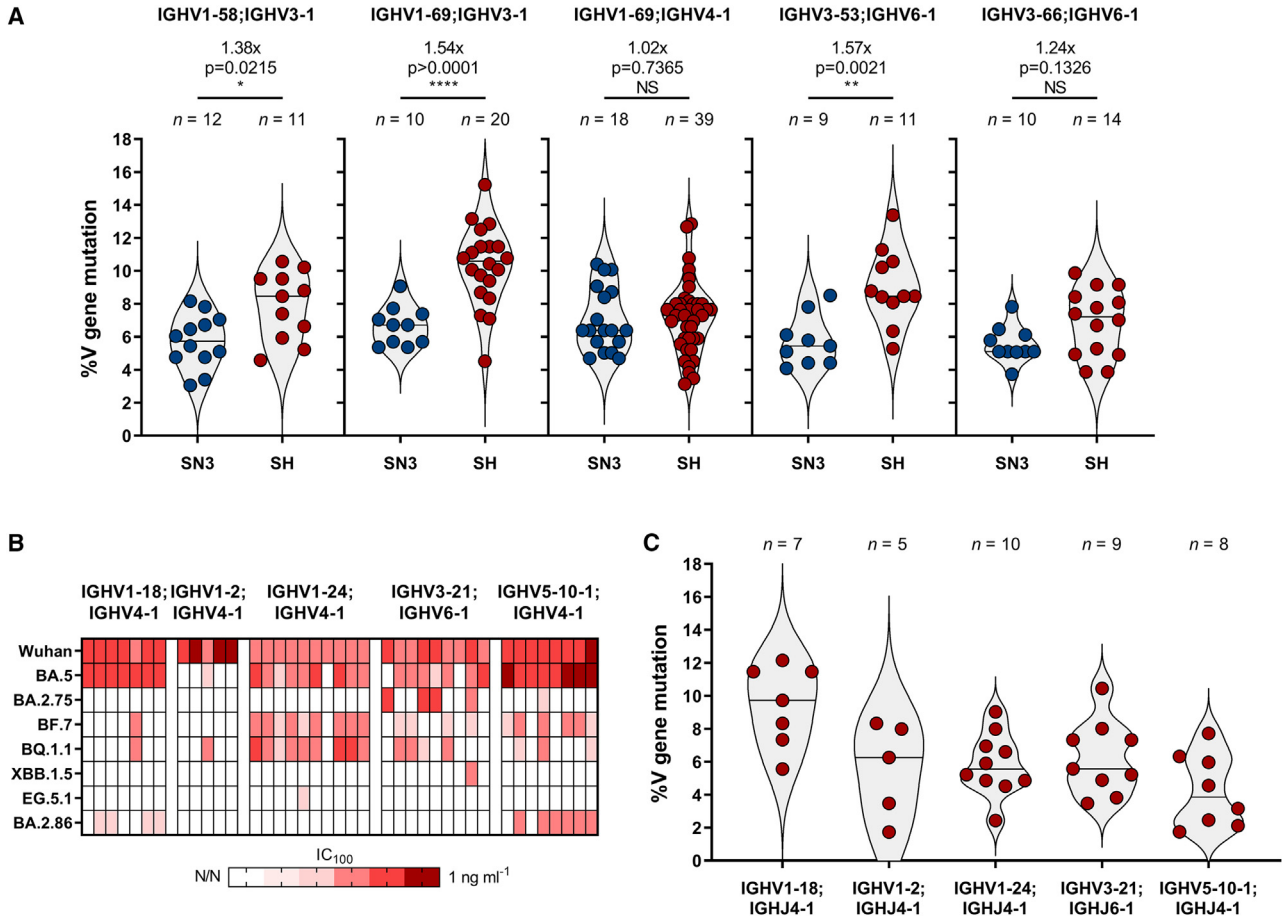

Figure 6. Characterization of SN3-SH shared germ lines and SH-exclusive germ lines

(A) The violin plots show the V gene somatic mutation frequency of IGHV1-24;IGHJ6-1, IGHV1-58;IGHJ3-1, IGHV3-53;IGHJ6-1, IGHV3-66;IGHJ4-1, and IGHV3-66;IGHJ6-1 gene-derived nAbs. The number of nAbs for each germ line and fold change are denoted on each graph. Violin plots show the median of V gene mutations. A nonparametric Mann-Whitney t test was used to evaluate statistical significances between groups. Two-tailed *p* value significances are shown as $^{*}p < 0.05$, $^{**}p < 0.01$, and $^{***}p < 0.0001$. Not significant *p* values were denoted on the figure as "NS."

(B) The heatmap shows the IC_{100} of germ lines found in SH but not in SN3 against all SARS-CoV-2 variants tested in this study.

(C) The violin plot shows the V gene somatic mutation frequency of selected germ lines found exclusively in the SH cohort. The number of nAbs for each germ line is denoted on each graph. Violin plots show the mean of V gene mutations.

policymakers on the use of heterologous vaccination strategies to induce broad and variant resistant antibody immunity.

Limitations of the study

The limitation of this study is the small sample size used to investigate the importance of reported B cell germ lines and the evolution of the antibody compartment. However, the predominance and importance of the B cell germ lines highlighted in this work have been reported in different geographies from Europe, North America, and Asia,[7,43–45] and following SARS-CoV-2 infection or immunization with mRNA, adenoviral, or inactivated COVID-19 vaccines.[7,46,47] The public relevance of these germ lines mitigates the limitation of this work. Another limitation of this work is the use of the Wuhan S protein as the only probe for SARS-CoV-2-specific B cells, which may have limited information on Omicron *de novo* B cell response. However, recent findings have demonstrated that Omicron-specific *de novo* antibody response accounts for less than 1% of total antibodies after breakthrough infection.[48] Therefore, our analysis has captured the almost totality of the antibody response, and our observations and conclusions can be extended on the impact of the original antigenic sin on the B cell and antibody response.

STAR★METHODS

Detailed methods are provided in the online version of this paper and include the following:

- KEY RESOURCES TABLE
- RESOURCE AVAILABILITY
  - Lead contact
  - Materials availability
  - Data and code availability
- EXPERIMENTAL MODEL AND STUDY PARTICIPANT DETAILS
  - Ethics and enrollment of donors with super hybrid immunity
  - Viral strains and cell culture

SUPPLEMENTAL INFORMATION

Supplemental information can be found online at https://doi.org/10.1016/j.celrep.2024.114645.

ACKNOWLEDGMENTS

This work received funding from the European Research Council (ERC) advanced grant (agreement no. 101098201 [PROACTIVE]). P.M. acknowledges support from the Research Foundation Flanders (COVID-19 research grant G0H4420N) and Internal Funds KU Leuven (grant 3M170314). Work in the laboratory of O.S. is funded by Institut Pasteur, Urgence COVID-19 Fundraising Campaign of Institut Pasteur, Fondation pour la Recherche Médicale (FRM), ANRS, the Vaccine Research Institute (ANR-10- LABX-77), Labex IBEID (ANR-10-LABX-62-IBEID), ANR/FRM Flash Covid PROTEO-SARS-CoV-2, ANR Coronamito, HERA European funding, Sanofi, and IDISCOVR. The laboratory of E.S.-L. is funded by Institut Pasteur, the INCEPTION program (Investissements d'Avenir grant ANR-16-CONV-0005), the Labex IBEID (grant no. ANR-10-LABX-62-IBEID), the HERA Project DURABLE (grant no 101102733), and the NIH PICREID (grant no. U01AI151758). N.T. and M.M.N. acknowledge support from Wellcome Trust 360G-Wellcome-220981_Z_20_Z.

AUTHOR CONTRIBUTIONS

Study conception: R.R. and E.A. Provided peripheral blood mononuclear cells (PBMCs) and enrolled SH donors: S.P., M.F., I.R., M.T., and F.M. Isolated PBMCs and performed single-cell sorting: I.P. Provided SARS-CoV-2 viruses: P.M., E.S.-L., and O.S. Expanded and titrated SARS-CoV-2 variants: G.P. Performed neutralization assays in BSL3 facilities: I.P., G.P., E.P., and G.A. SARS-CoV-1 and h-CoV pseudotype production and neutralization assay: E.P. and M.M.N. Expression of recombinant S proteins: E.P. and G.A. Performed antibody expression: I.P., G.A., G.R., and F.P. Performed ELISA assay on SARS-CoV-1, SARS-CoV-2, and h-CoV S proteins, and SARS-CoV-2 domains: G.P. and G.A. Performed epitope mapping: I.P. Performed ADCP and ADCD assays: I.P. Recovered variable regions of heavy (VH) and light (VL) regions of immunoglobulin molecule sequences and performed the repertoire analyses: P.P., G.M., D.C., and E.A. Manuscript writing: R.R. and E.A. Final revision of the manuscript: I.P., G.P., E.P., G.A., P.P., G.M., D.C., G.R., F.P., M.M.N., S.P., M.F., I.R., M.T., F.M., D.M., P.M., N.T., O.S., R.R. and E.A. Project coordination: E.A.

DECLARATION OF INTERESTS

I.P., G.P., E.P., P.P., R.R., and E.A. are listed as inventors of full-length human mAbs described in Italian patent application nos. 102020000015754 filed on June 30, 2020, 102020000018955 filed on August 3, 2020, and 102020000029969 filed on December 4, 2020, and the international patent system no. PCT/IB2021/055755 filed on June 28, 2021. I.P., E.P., G.A., P.P., R.R., and E.A. are listed as inventors of full-length human mAbs described in the international patent system no. PCT/IB2022/061257 filed on November 22, 2022. All patents were submitted by Fondazione Toscana Life Sciences, Siena, Italy.

Received: April 29, 2024
Revised: July 19, 2024
Accepted: July 31, 2024

REFERENCES

1. (ECDC), E.C.f.D.P.a.C. (2024). SARS-CoV-2 Variants of Concern as of 2 February 2024.
2. Andreano, E., and Rappuoli, R. (2021). Immunodominant antibody germlines in COVID-19. J. Exp. Med. *218*, e20210281. https://doi.org/10.1084/jem.20210281.
3. Fagiani, F., Catanzaro, M., and Lanni, C. (2020). Molecular features of IGHV3-53-encoded antibodies elicited by SARS-CoV-2. Signal Transduct. Targeted Ther. *5*, 170. https://doi.org/10.1038/s41392-020-00287-4.
4. Wang, E.Y., Mao, T., Klein, J., Dai, Y., Huck, J.D., Jaycox, J.R., Liu, F., Zhou, T., Israelow, B., Wong, P., et al. (2021). Diverse functional autoantibodies in patients with COVID-19. Nature *595*, 283–288. https://doi.org/10.1038/s41586-021-03631-y.
5. Robbiani, D.F., Gaebler, C., Muecksch, F., Lorenzi, J.C.C., Wang, Z., Cho, A., Agudelo, M., Barnes, C.O., Gazumyan, A., Finkin, S., et al. (2020). Convergent antibody responses to SARS-CoV-2 in convalescent individuals. Nature *584*, 437–442. https://doi.org/10.1038/s41586-020-2456-9.
6. Andreano, E., Nicastri, E., Paciello, I., Pileri, P., Manganaro, N., Piccini, G., Manenti, A., Pantano, E., Kabanova, A., Troisi, M., et al. (2021). Extremely potent human monoclonal antibodies from COVID-19 convalescent patients. Cell *184*, 1821–1835.e16. https://doi.org/10.1016/j.cell.2021.02.035.
7. Andreano, E., Paciello, I., Piccini, G., Manganaro, N., Pileri, P., Hyseni, I., Leonardi, M., Pantano, E., Abbiento, V., Benincasa, L., et al. (2021). Hybrid immunity improves B cells and antibodies against SARS-CoV-2 variants. Nature *600*, 530–535. https://doi.org/10.1038/s41586-021-04117-7.
8. Yuan, M., Liu, H., Wu, N.C., Lee, C.-C.D., Zhu, X., Zhao, F., Huang, D., Yu, W., Hua, Y., Tien, H., et al. (2020). Structural basis of a shared antibody response to SARS-CoV-2. Science (New York, N.Y.) *369*, 1119–1123. https://doi.org/10.1126/science.abd2321.
9. Callaway, E. (2021). Coronavirus variants get Greek names - but will scientists use them? Nature *594*, 162. https://doi.org/10.1038/d41586-021-01483-0.
10. Piccoli, L., Park, Y.-J., Tortorici, M.A., Czudnochowski, N., Walls, A.C., Beltramello, M., Silacci-Fregni, C., Pinto, D., Rosen, L.E., Bowen, J.E., et al. (2020). Mapping Neutralizing and Immunodominant Sites on the SARS-CoV-2 Spike Receptor-Binding Domain by Structure-Guided High-Resolution Serology. Cell *183*, 1024–1042.e21. https://doi.org/10.1016/j.cell.2020.09.037.
11. Karim, S.S.A., and Karim, Q.A. (2021). Omicron SARS-CoV-2 variant: a new chapter in the COVID-19 pandemic. Lancet (London, England) *398*, 2126–2128. https://doi.org/10.1016/s0140-6736(21)02758-6.
12. Viana, R., Moyo, S., Amoako, D.G., Tegally, H., Scheepers, C., Althaus, C.L., Anyaneji, U.J., Bester, P.A., Boni, M.F., Chand, M., et al. (2022). Rapid epidemic expansion of the SARS-CoV-2 Omicron variant in southern Africa. Nature *603*, 679–686. https://doi.org/10.1038/s41586-022-04411-y.
13. Andreano, E., Paciello, I., Marchese, S., Donnici, L., Pierleoni, G., Piccini, G., Manganaro, N., Pantano, E., Abbiento, V., Pileri, P., et al. (2022). Anatomy of Omicron BA.1 and BA.2 neutralizing antibodies in COVID-19 mRNA vaccinees. Nat. Commun. *13*, 3375. https://doi.org/10.1038/s41467-022-31115-8.

14. Andreano, E., Paciello, I., Pierleoni, G., Piccini, G., Abbiento, V., Antonelli, G., Pileri, P., Manganaro, N., Pantano, E., Maccari, G., et al. (2023). B cell analyses after SARS-CoV-2 mRNA third vaccination reveals a hybrid immunity like antibody response. Nat. Commun. *14*, 53. https://doi.org/10.1038/s41467-022-35781-6.

15. Yu, J., Collier, A.-r.Y., Rowe, M., Mardas, F., Ventura, J.D., Wan, H., Miller, J., Powers, O., Chung, B., Siamatu, M., et al. (2022). Neutralization of the SARS-CoV-2 Omicron BA.1 and BA.2 Variants. N. Engl. J. Med. *386*, 1579–1580. https://doi.org/10.1056/NEJMc2201849.

16. Ai, J., Wang, X., He, X., Zhao, X., Zhang, Y., Jiang, Y., Li, M., Cui, Y., Chen, Y., Qiao, R., et al. (2022). Antibody evasion of SARS-CoV-2 Omicron BA.1, BA.1.1, BA.2, and BA.3 sub-lineages. Cell Host Microbe *30*, 1077–1083.e4. https://doi.org/10.1016/j.chom.2022.05.001.

17. Khare, S., Gurry, C., Freitas, L., Schultz, M.B., Bach, G., Diallo, A., Akite, N., Ho, J., Lee, R.T., Yeo, W., et al. (2021). GISAID's Role in Pandemic Response. China CDC Wkly. *3*, 1049–1051. https://doi.org/10.46234/ccdcw2021.255.

18. Meo, S.A., Meo, A.S., and Klonoff, D.C. (2023). Omicron new variant BA.2.86 (Pirola): Epidemiological, biological, and clinical characteristics - a global data-based analysis. Eur. Rev. Med. Pharmacol. Sci. *27*, 9470–9476. https://doi.org/10.26355/eurrev_202310_33975.

19. Wang, Q., Guo, Y., Liu, L., Schwanz, L.T., Li, Z., Nair, M.S., Ho, J., Zhang, R.M., Iketani, S., Yu, J., et al. (2023). Antigenicity and receptor affinity of SARS-CoV-2 BA.2.86 spike. Nature *624*, 639–644. https://doi.org/10.1038/s41586-023-06750-w.

20. Wang, Q., Guo, Y., Zhang, R.M., Ho, J., Mohri, H., Valdez, R., Manthei, D.M., Gordon, A., Liu, L., and Ho, D.D. (2023). Antibody neutralisation of emerging SARS-CoV-2 subvariants: EG.5.1 and XBC.1.6. Lancet Infect. Dis. *23*, e397–e398. https://doi.org/10.1016/S1473-3099(23)00555-8.

21. Lassaunière, R., Polacek, C., Utko, M., Sørensen, K.M., Baig, S., Ellegaard, K., Escobar-Herrera, L.A., Fomsgaard, A., Spiess, K., Gunalan, V., et al. (2023). Virus isolation and neutralisation of SARS-CoV-2 variants BA.2.86 and EG.5.1. Lancet Infect. Dis. *23*, e509–e510. https://doi.org/10.1016/S1473-3099(23)00682-5.

22. Sheward, D.J., Kim, C., Fischbach, J., Sato, K., Muschiol, S., Ehling, R.A., Björkström, N.K., Karlsson Hedestam, G.B., Reddy, S.T., Albert, J., et al. (2022). Omicron sublineage BA.2.75.2 exhibits extensive escape from neutralising antibodies. Lancet Infect. Dis. *22*, 1538–1540. https://doi.org/10.1016/S1473-3099(22)00663-6.

23. Planas, D., Bruel, T., Staropoli, I., Guivel-Benhassine, F., Porrot, F., Maes, P., Grzelak, L., Prot, M., Mougari, S., Planchais, C., et al. (2023). Resistance of Omicron subvariants BA.2.75.2, BA.4.6, and BQ.1.1 to neutralizing antibodies. Nat. Commun. *14*, 824. https://doi.org/10.1038/s41467-023-36561-6.

24. Khan, K., Lustig, G., Römer, C., Reedoy, K., Jule, Z., Karim, F., Ganga, Y., Bernstein, M., Baig, Z., Jackson, L., et al. (2023). Evolution and neutralization escape of the SARS-CoV-2 BA.2.86 subvariant. Nat. Commun. *14*, 8078. https://doi.org/10.1038/s41467-023-43703-3.

25. Andreano, E., Paciello, I., Pierleoni, G., Maccari, G., Antonelli, G., Abbiento, V., Pileri, P., Benincasa, L., Giglioli, G., Piccini, G., et al. (2023). mRNA vaccines and hybrid immunity use different B cell germlines against Omicron BA.4 and BA.5. Nat. Commun. *14*, 1734. https://doi.org/10.1038/s41467-023-37422-y.

26. Andreano, E., Paciello, I., Pierleoni, G., Piccini, G., Abbiento, V., Antonelli, G., Pileri, P., Manganaro, N., Pantano, E., Maccari, G., et al. (2022). COVID-19 mRNA third dose induces a unique hybrid immunity-like antibody response. Preprint at bioRxiv, 491201, 2022.2005.2009. https://doi.org/10.1101/2022.05.09.491201.

27. Rubin, R. (2024). As COVID-19 Cases Surge, Here's What to Know About JN.1, the Latest SARS-CoV-2 "Variant of Interest". JAMA *331*, 382–383. https://doi.org/10.1001/jama.2023.27841.

28. Torres, J.L., Ozorowski, G., Andreano, E., Liu, H., Copps, J., Piccini, G., Donnici, L., Conti, M., Planchais, C., Planas, D., et al. (2022). Structural insights of a highly potent pan-neutralizing SARS-CoV-2 human monoclonal antibody. Proc. Natl. Acad. Sci. USA *119*, e2120976119. https://doi.org/10.1073/pnas.2120976119.

29. Pinto, D., Park, Y.J., Beltramello, M., Walls, A.C., Tortorici, M.A., Bianchi, S., Jaconi, S., Culap, K., Zatta, F., De Marco, A., et al. (2020). Cross-neutralization of SARS-CoV-2 by a human monoclonal SARS-CoV antibody. Nature *583*, 290–295. https://doi.org/10.1038/s41586-020-2349-y.

30. Yuan, M., Wu, N.C., Zhu, X., Lee, C.-C.D., So, R.T.Y., Lv, H., Mok, C.K.P., and Wilson, I.A. (2020). A highly conserved cryptic epitope in the receptor binding domains of SARS-CoV-2 and SARS-CoV. Science (New York, N.Y.) *368*, 630–633. https://doi.org/10.1126/science.abb7269.

31. Chen, E.C., Gilchuk, P., Zost, S.J., Ilinykh, P.A., Binshtein, E., Huang, K., Myers, L., Bonissone, S., Day, S., Kona, C.R., et al. (2023). Systematic analysis of human antibody response to ebolavirus glycoprotein shows high prevalence of neutralizing public clonotypes. Cell Rep. *42*, 112370. https://doi.org/10.1016/j.celrep.2023.112370.

32. Zhang, Q., Ju, B., Ge, J., Chan, J.F.-W., Cheng, L., Wang, R., Huang, W., Fang, M., Chen, P., Zhou, B., et al. (2021). Potent and protective IGHV3-53/3-66 public antibodies and their shared escape mutant on the spike of SARS-CoV-2. Nat. Commun. *12*, 4210. https://doi.org/10.1038/s41467-021-24514-w.

33. Hansen, J., Baum, A., Pascal, K.E., Russo, V., Giordano, S., Wloga, E., Fulton, B.O., Yan, Y., Koon, K., Patel, K., et al. (2020). Studies in humanized mice and convalescent humans yield a SARS-CoV-2 antibody cocktail. Science (New York, N.Y.) *369*, 1010–1014. https://doi.org/10.1126/science.abd0827.

34. Tortorici, M.A., Addetia, A., Seo, A.J., Brown, J., Sprouse, K., Logue, J., Clark, E., Franko, N., Chu, H., and Veesler, D. (2024). Persistent immune imprinting occurs after vaccination with the COVID-19 XBB.1.5 mRNA booster in humans. Immunity *57*, 904–911.e4. https://doi.org/10.1016/j.immuni.2024.02.016.

35. Yisimayi, A., Song, W., Wang, J., Jian, F., Yu, Y., Chen, X., Xu, Y., Yang, S., Niu, X., Xiao, T., et al. (2024). Repeated Omicron exposures override ancestral SARS-CoV-2 immune imprinting. Nature *625*, 148–156. https://doi.org/10.1038/s41586-023-06753-7.

36. Qu, P., Xu, K., Faraone, J.N., Goodarzi, N., Zheng, Y.M., Carlin, C., Bednash, J.S., Horowitz, J.C., Mallampalli, R.K., Saif, L.J., et al. (2024). Immune evasion, infectivity, and fusogenicity of SARS-CoV-2 BA.2.86 and FLip variants. Cell *187*, 585–595.e6. https://doi.org/10.1016/j.cell.2023.12.026.

37. Zhang, L., Kempf, A., Nehlmeier, I., Cossmann, A., Richter, A., Bdeir, N., Graichen, L., Moldenhauer, A.S., Dopfer-Jablonka, A., Stankov, M.V., et al. (2024). SARS-CoV-2 BA.2.86 enters lung cells and evades neutralizing antibodies with high efficiency. Cell *187*, 596–608.e17. https://doi.org/10.1016/j.cell.2023.12.025.

38. Wang, X., Lu, L., and Jiang, S. (2024). SARS-CoV-2 evolution from the BA.2.86 to JN.1 variants: unexpected consequences. Trends Immunol. *45*, 81–84. https://doi.org/10.1016/j.it.2024.01.003.

39. Delphine, P., Isabelle, S., Vincent, M., Frederic, L., Flora, D., Matthieu, P., Francoise, P., Florence, G.-B., Banujaa, J., Angela, B., et al. (2024). Distinct evolution of SARS-CoV-2 Omicron XBB and BA.2.86/JN.1 lineages combining increased fitness and antibody evasion. Preprint at bioRxiv, 567873, 2023.2011.2020. https://doi.org/10.1101/2023.11.20.567873.

40. Yang, S., Yu, Y., Xu, Y., Jian, F., Song, W., Yisimayi, A., Wang, P., Wang, J., Liu, J., Yu, L., et al. (2024). Fast evolution of SARS-CoV-2 BA.2.86 to JN.1 under heavy immune pressure. Lancet Infect. Dis. *24*, e70–e72. https://doi.org/10.1016/S1473-3099(23)00744-2.

41. Liang, C.-Y., Raju, S., Liu, Z., Li, Y., Asthagiri Arunkumar, G., Case, J.B., Scheaffer, S.M., Zost, S.J., Acreman, C.M., Gagne, M., et al. (2024). Imprinting of serum neutralizing antibodies by Wuhan-1 mRNA vaccines. Nature *630*, 950–960. https://doi.org/10.1038/s41586-024-07539-1.

42. Alsoussi, W.B., Malladi, S.K., Zhou, J.Q., Liu, Z., Ying, B., Kim, W., Schmitz, A.J., Lei, T., Horvath, S.C., Sturtz, A.J., et al. (2023). SARS-CoV-2 Omicron boosting induces de novo B cell response in humans. Nature *617*, 592–598. https://doi.org/10.1038/s41586-023-06025-4.

43. Kaku, C.I., Bergeron, A.J., Ahlm, C., Normark, J., Sakharkar, M., Forsell, M.N.E., and Walker, L.M. (2022). Recall of preexisting cross-reactive B cell memory after Omicron BA.1 breakthrough infection. Sci. Immunol. *7*, eabq3511. https://doi.org/10.1126/sciimmunol.abq3511.

44. Kaku, C.I., Starr, T.N., Zhou, P., Dugan, H.L., Khalifé, P., Song, G., Champney, E.R., Mielcarz, D.W., Geoghegan, J.C., Burton, D.R., et al. (2023). Evolution of antibody immunity following Omicron BA.1 breakthrough infection. Nat. Commun. *14*, 2751. https://doi.org/10.1038/s41467-023-38345-4.

45. Li, L., Chen, X., Wang, Z., Li, Y., Wang, C., Jiang, L., and Zuo, T. (2023). Breakthrough infection elicits hypermutated IGHV3-53/3-66 public antibodies with broad and potent neutralizing activity against SARS-CoV-2 variants including the emerging EG.5 lineages. PLoS Pathog. *19*, e1011856. https://doi.org/10.1371/journal.ppat.1011856.

46. Liu, Y., Wang, Z., Zhuang, X., Zhang, S., Chen, Z., Zou, Y., Sheng, J., Li, T., Tai, W., Yu, J., et al. (2023). Inactivated vaccine-elicited potent antibodies can broadly neutralize SARS-CoV-2 circulating variants. Nat. Commun. *14*, 2179. https://doi.org/10.1038/s41467-023-37926-7.

47. Seow, J., Graham, C., Hallett, S.R., Lechmere, T., Maguire, T.J.A., Huettner, I., Cox, D., Khan, H., Pickering, S., Roberts, R., et al. (2022). ChAdOx1 nCoV-19 vaccine elicits monoclonal antibodies with cross-neutralizing activity against SARS-CoV-2 viral variants. Cell Rep. *39*, 110757. https://doi.org/10.1016/j.celrep.2022.110757.

48. Johnston, T.S., Li, S.H., Painter, M.M., Atkinson, R.K., Douek, N.R., Reeg, D.B., Douek, D.C., Wherry, E.J., and Hensley, S.E. (2024). Immunological imprinting shapes the specificity of human antibody responses against SARS-CoV-2 variants. Immunity *57*, 912–925.e4. https://doi.org/10.1016/j.immuni.2024.02.017.

49. Tiller, T., Meffre, E., Yurasov, S., Tsuiji, M., Nussenzweig, M.C., and Wardemann, H. (2008). Efficient generation of monoclonal antibodies from single human B cells by single cell RT-PCR and expression vector cloning. J. Immunol. Methods *329*, 112–124. https://doi.org/10.1016/j.jim.2007.09.017.

50. Wrapp, D., Wang, N., Corbett, K.S., Goldsmith, J.A., Hsieh, C.-L., Abiona, O., Graham, B.S., and McLellan, J.S. (2020). Cryo-EM structure of the 2019-nCoV spike in the prefusion conformation. Science (New York, N.Y.) *367*, 1260–1263. https://doi.org/10.1126/science.abb2507.

51. Carnell, G., Grehan, K., Ferrara, F., Molesti, E., and Temperton, N. (2017). An Optimized Method for the Production Using PEI, Titration and Neutralizationof SARS-CoV Spike Luciferase Pseudotypes. Bio. Protoc. *7*, e2514. https://doi.org/10.21769/BioProtoc.2514.

52. Grehan, K., Ferrara, F., and Temperton, N. (2015). An optimised method for the production of MERS-CoV spike expressing viral pseudotypes. MethodsX *2*, 379–384. https://doi.org/10.1016/j.mex.2015.09.003.

53. Carnell, G.W., Ferrara, F., Grehan, K., Thompson, C.P., and Temperton, N.J. (2015). Pseudotype-based neutralization assays for influenza: a systematic analysis. Front. Immunol. *6*, 161. https://doi.org/10.3389/fimmu.2015.00161.

54. Huang, J., Doria-Rose, N.A., Longo, N.S., Laub, L., Lin, C.L., Turk, E., Kang, B.H., Migueles, S.A., Bailer, R.T., Mascola, J.R., and Connors, M. (2013). Isolation of human monoclonal antibodies from peripheral blood B cells. Nat. Protoc. *8*, 1907–1915. https://doi.org/10.1038/nprot.2013.117.

55. Notarbartolo, S., Ranzani, V., Bandera, A., Gruarin, P., Bevilacqua, V., Putignano, A.R., Gobbini, A., Galeota, E., Manara, C., Bombaci, M., et al. (2021). Integrated longitudinal immunophenotypic, transcriptional and repertoire analyses delineate immune responses in COVID-19 patients. Sci. Immunol. *6*, eabg5021. https://doi.org/10.1126/sciimmunol.abg5021.

56. Conforti, A., Marra, E., Palombo, F., Roscilli, G., Ravà, M., Fumagalli, V., Muzi, A., Maffei, M., Luberto, L., Lione, L., et al. (2022). COVID-eVax, an electroporated DNA vaccine candidate encoding the SARS-CoV-2 RBD, elicits protective responses in animal models. Mol. Ther. *30*, 311–326. https://doi.org/10.1016/j.ymthe.2021.09.011.

57. Paciello, I., Maccari, G., Pantano, E., Andreano, E., and Rappuoli, R. (2024). High-resolution map of the Fc functions mediated by COVID-19-neutralizing antibodies. Proc. Natl. Acad. Sci. USA *121*, e2314730121. https://doi.org/10.1073/pnas.2314730121.

58. Kepler, T.B. (2013). Reconstructing a B-cell clonal lineage. I. Statistical inference of unobserved ancestors. F1000Res. *2*, 103. https://doi.org/10.12688/f1000research.2-103.v1.

59. Kepler, T.B., Munshaw, S., Wiehe, K., Zhang, R., Yu, J.-S., Woods, C.W., Denny, T.N., Tomaras, G.D., Alam, S.M., Moody, M.A., et al. (2014). Reconstructing a B-Cell Clonal Lineage. II. Front. Immunol., Mutation, Selection, and Affinity Maturation. Front. Immunol. *5*, 170. https://doi.org/10.3389/fimmu.2014.00170.

STAR★METHODS

KEY RESOURCES TABLE

REAGENT or RESOURCE	SOURCE	IDENTIFIER
Antibodies		
CD19 V421	BD Biosciences	Cat#562440
IgM PerCP-Cy5.5	BD Biosciences	Cat#561285
CD27 PE	BD Biosciences	Cat#340425
IgD-A700	BD Biosciences	Cat#561302
CD3 PE-Cy7	BioLegend	Cat#300420
CD14 PE-Cy7	BioLegend	Cat#301814
CD56 PECy7	Biolegend	Cat#318318
Strep-Tactin™XT DY-649	iba-lifesciences	Cat#2-1568-050
Strep-TactinXT DY-488	iba-lifesciences	Cat#2-1562-050
Live/Dead Fixable Aqua	Invitrogen™	Cat# L34957
goat anti-rabbit antibody against C3-FITC	MP Biomedicals	Cat# 0855654
Goat Anti-Human IgA-UNLB	Southern Biotech	Cat#2050-01
Goat Anti-Human IgA-Alkaline Phosphatase	Southern Biotech	Cat#2050-04
Human IgA-UNLB	Southern Biotech	Cat# 0155L-01
Human IgG-UNLB	Southern Biotech	Cat# 0150-01
Goat Anti-Human IgG-UNLB	Southern Biotech	Cat#2040-01
Goat Anti-Human IgG-AP	Southern Biotech	Cat#2040-04
Bacterial and virus strains		
SARS-CoV-2 wild type	EVAg	GenBank: MT066156
SARS-CoV-2 BA.5	KU Leuven, Rega Institute, Clinical and Epidemiological Virology, Leuven, Belgium	GISAID ID: EPI_ISL_13389618
SARS-CoV-2 BA.2.75	KU Leuven, Rega Institute, Clinical and Epidemiological Virology, Leuven, Belgium	GISAID ID: EPI_ISL_14732896
SARS-CoV-2 BF.7	KU Leuven, Rega Institute, Clinical and Epidemiological Virology, Leuven, Belgium	GISAID ID: EPI_ISL_13499917
SARS-CoV-2 BQ.1.1	KU Leuven, Rega Institute, Clinical and Epidemiological Virology, Leuven, Belgium	GISAID ID: EPI_ISL_15455664
SARS-CoV-2 XBB.1.5	KU Leuven, Rega Institute, Clinical and Epidemiological Virology, Leuven, Belgium	GISAID ID: EPI_ISL_17272995
SARS-CoV-2 EG.5.1.1	KU Leuven, Rega Institute, Clinical and Epidemiological Virology, Leuven, Belgium	GISAID ID: EPI_ISL_18245523
SARS-CoV-2 BA.2.86	National Reference Center for Viruses of Respiratory Infections, Institut Pasteur, Paris, France	GISAID ID: EPI_ISL_18221650
Biological samples		
PBMCs and IgGs of donor SN2_PT-001	Andreano et al.[7]	N/A
PBMCs and IgGs of donor SN2_PT-002	Andreano et al.[7]	N/A
PBMCs and IgGs of donor SP2_PT-003	Andreano et al.[7]	N/A
PBMCs and IgGs of donor SP2_PT-004	Andreano et al.[7]	N/A
PBMCs and IgGs of donor SP2_PT-005	Andreano et al.[7]	N/A

(*Continued on next page*)

Continued

REAGENT or RESOURCE	SOURCE	IDENTIFIER
PBMCs and IgGs of donor SP2_PT-006	Andreano et al.[7]	N/A
PBMCs and IgGs of donor SN2_PT-007	Andreano et al.[7]	N/A
PBMCs and IgGs of donor SN2_PT-008	Andreano et al.[7]	N/A
PBMCs and IgGs of donor SP2_PT-009	Andreano et al.[7]	N/A
PBMCs and IgGs of donor SN2_PT-010	Andreano et al.[7]	N/A
PBMCs and IgGs of donor SN3_PT-001	Andreano et al.[14]	N/A
PBMCs and IgGs of donor SN3_PT-002	Andreano et al.[14]	N/A
PBMCs and IgGs of donor SN3_PT-008	Andreano et al.[14]	N/A
PBMCs and IgGs of donor SN3_PT-010	Andreano et al.[14]	N/A
PBMCs and IgGs of donor SH_PT-004	This paper	N/A
PBMCs and IgGs of donor SH_PT-009	This paper	N/A
PBMCs and IgGs of donor SH_PT-011	This paper	N/A
PBMCs and IgGs of donor SH_PT-012	This paper	N/A
PBMCs and IgGs of donor SH_PT-013	This paper	N/A
PBMCs and IgGs of donor SH_PT-014	This paper	N/A
Chemicals, peptides, and recombinant proteins		
Fetal Bovine Serum (FBS) Hyclone	Sigma-Aldrich	Cat#D2650
Fetal Bovine Serum (FBS) heat inactivated	Gibco™	Cat# 10500-064
DPBS, no calcium, no magnesium	Gibco™	Cat#14190144
Baby Rabbit Complement	Tissue Culture Grade	Cat# CL3441
Normal rabbit serum	Life technologies	Cat# 31883
DMSO	Sigma-Aldrich	Cat#D2650
DNase I	Roche	Cat# 11284932001
RNaseOUT Recombinant Ribonuclease Inhibitor	Thermo Fisher	Cat#10777-019
SuperScript IV Reverse Transcriptase	Thermo Fisher	Cat#18091200
Ultra Pure Bovine serum albumin (BSA)	Thermo Fisher	Cat#AM2618
DEPC-Treated water	Thermo Fisher	Cat#AM9916
dNTP Set (100 mM)	Thermo Fisher	Cat#10297018
MgCl2 Magnesium Chloride 25mM	Thermo Fisher	Cat#AB0359
Kapa Long Range Polymerase	Sigma-Aldrich	Cat#KK3005
NEBuilder® HiFi DNA Assembly Master Mix	New England BioLabs	Cat#E2621X
Q5® High-Fidelity DNA Polymerases	New England BioLabs	Cat#M0491L
Expi293™ Expression Medium	Thermo Fisher	Cat#A1435101
ExpiCHO™ Expression Medium	Thermo Fisher	Cat# A2910001
ExpiFectamine™ 293 Transfection Kit	Thermo Fisher	Cat#A14524
ExpiFectamine™ CHO Transfection Kit	Thermo Fisher	Cat# A29129
DMEM high Glucose	Thermo Fisher	Cat#11965092
Pen strep glutamine 100X	Gibco™	Cat#10378-016
HEPES	Gibco™	Cat#15630-080
Sodium Pyruvate	Gibco™	Cat# 11360-070
Non-Essential Amino Acids	Gibco™	Cat# 11140050
Ficoll-Paque™ PREMIUM	Sigma-Aldrich	Cat#GE17-5442-03
MycoZap Plus-PR	Lonza	Cat#VZA2022
IMDM with GlutaMAX	Thermo Fisher	Cat# 31980048
Benzonase Nuclease	Sigma-Aldrich	Cat#70664-3
IL-2 Recombinant Human Protein	Thermo Fisher	Cat#PHC0023
IL-21 Recombinant Human Protein	Thermo Fisher	Cat#PHC0211
Slide-A-Lyzer™ Dialysis Cassettes	Thermo Fisher	Cat#66003

(*Continued on next page*)

Continued

REAGENT or RESOURCE	SOURCE	IDENTIFIER
HiTrap Protein G HP column	Cytiva	Cat#17040503
HisTrap FF Crude column	Cytiva	Cat#17528601
Bovine Serum Albumin	Sigma	Cat# A2153
TMB HRP Microwell substrate	BETHYL	Cat# E102
Alkaline Phosphatase Yellow (pNPP)	Sigma-Aldrich	Cat# P7998
IgG-Peroxidase antibody	Sigma-Aldrich	Cat# A0293
True Nuclear Transcription Factor Buffet set	BioLegend	Cat# 424401
Tween 20	VWR	Cat#A4974.0250
Critical commercial assays		
ELISA Starter Accessory Kit	Bethyl Laboratories	Cat#E101
Alexa Fluor™ 488 NHS Ester	Invitrogen™	Cat#A20100
Alexa Fluor™ 647 NHS Ester	Invitrogen™	Cat#A20006
Alexa Fluor™ 594 NHS Ester	Invitrogen™	Cat#A20004
Zeba™ Spin Desalting Columns	Thermo Scientific™	Cat#89890
Dynabeads™ His-Tag	Invitrogen™	Cat#10103D
Bright-Glo Luciferase Assay System	Promega	Cat# E2620
Pierce BCA Protein Assay Kit	Thermo Fisher	Cat#23227
Deposited data		
Sequences of SARS-CoV-2-neutralizing antibodies	This paper	https://github.com/dasch-lab/SARS-CoV-2_superhybrid
Experimental models: cell lines		
VERO E6 cell line	ATCC	Cat#CRL-1586
Expi293F™ cells	Gibco™	Cat#A14527
THP-1	ATCC	Cat#IB-202
ExpiCHO-S™ Cells	Gibco™	Cat# A29127
HEK293TN-hACE2	System Bioscience	Cat# LV900A-1
HUH7 cell line	Japanese Collection of Research Bioresources (JCRB)	JCRB-0403
CHO-K1 cell line	ATCC	CCL-61
HEKTN/17 cell line	ATCC	CRL-11268
3T3-msCD40L Cells	NIH AIDS Reagent Program	Cat#12535
Oligonucleotides		
Single cell PCR Primer	This paper	N/A
Random Hexamer Primer	Thermo Fisher	Cat#SO142
TAP forward primer (TTAGGCACCCCAGGCTTTAC)	This paper	N/A
TAP forward primer (AGATGGTTCTTTCCGCCTCA)	This paper	N/A
Recombinant DNA		
Human antibody expression vectors (IgG1, Igl, Igk)	Tiller et al.[49]	N/A
Plasmid encoding SARS-CoV-2 S ectodomain (amino acids 1–1208 of SARS-CoV-2 S; GenBank: MN908947)	Wrapp et al.[50]	N/A
Plasmid encoding SARS-CoV-2 RBD (amino acids 319–591 of SARS-CoV-2 S; GenBank: MN908947)	Jason McLellan Lab	N/A
pCDNA3.1+-SARS-CoV-2 Spike from Wuhan-Hu-1 isolate (GenBank MN908947.3) codon optimised	Andreano et al.[6]	pCDNA-S2
pCAGGS-SARS-CoV-2 Spike from Wuhan-Hu-1 isolate (GenBank MN908947.3) encoding D614G mutation and codon optimised	Andreano et al.[6]	pCAGGS-S2 D614G

(*Continued on next page*)

Continued

REAGENT or RESOURCE	SOURCE	IDENTIFIER
pCAGGS-SARS1 Spike protein codon optimised	Carnell et al.[51]	pCAGGS-S1
pCAGGS-MERS Spike protein codon optimised	Grehan et al.[52]	pCAGGS-MERS
229E SPIKE plasmid pcDNA3.1	Viral Pseudotype Unit, University of Kent	N/A
OC43 SPIKE plasmid pcDNA3.1	Viral Pseudotype Unit, University of Kent	N/A
HKU1 SPIKE plasmid pcDNA3.1	Viral Pseudotype Unit, University of Kent	N/A
pCSFLW Firefly luciferase encoding plasmid	Carnell et al.[53]	pCSFLW
SARS-CoV1 SPIKE plasmid pcDNA3.3_CoV1_D28	Addgene	#170447
p8.91 HIV Gag/Pol-encoding plasmid	Carnell et al.[53]	p8.91
Software and algorithms		
Prism 8	GraphPad	https://www.graphpad.com/
FlowJo 10.5.3	FlowJo, LLC	https://www.flowjo.com
Cloanalyst	BU, Computational Immunology	http://www.bu.edu/computationalimmunology/research/software/
R package stringdistm v0.9.8	CRAN	https://cran.r-project.org/web/packages/stringdist/index.html
R package ggraph v2.0.5	CRAN	https://ggraph.data-imaginist.com/index.html
ggplot2 v3.3.5	ggplot2	https://ggplot2.tidyverse.org/index.html
Matplotlib v3.2.2	NumFOCUS	https://matplotlib.org
pandas v1.3.5	NumFOCUS	https://pandas.pydata.org
Python v3.7.12	Python Software Foundation	https://www.python.org
FACSDiva	BD Bioscences	https://www.bdbiosciences.com
Other		
BD FACSAria™ Fusion	BD Biosciences	https://www.bdbiosciences.com
BD FACSymphony™ A3	BD Biosciences	https://www.bdbiosciences.com
Leica DMI-microscope	Leica Biosystem	https://www.leica-microsystems.com
LUNA-II Automated Cell Counter	Logo Biosystems	https://logosbio.com
Qubit Fluorometric Quantification	Thermo Fisher	https://www.thermofisher.com
ÄKTA go	Cytiva Lifesciences	https://www.cytivalifesciences.com
GloMax Luminometer	Promega	https://ita.promega.com
Varioskan LUX multimode microplate reader	Thermo Fisher	https://www.thermofisher.com

RESOURCE AVAILABILITY

Lead contact

Further information and requests for resources and reagents should be directed to and will be fulfilled by the lead contact, Emanuele Andreano (e.andreano@toscanalifesciences.org).

Materials availability

Reagents generated in this study are available from the lead contact with a completed Materials Transfer Agreement.

Data and code availability

- All data supporting the findings in this study are available within the article or can be obtained from the lead contact upon request. Sequences data are publicly available on GitHub: https://github.com/dasch-lab/SARS-CoV-2_superhybrid
- This paper does not report original code.
- Any additional information required to reanalyze the data reported in this paper is available from the lead contact upon request.

EXPERIMENTAL MODEL AND STUDY PARTICIPANT DETAILS

Ethics and enrollment of donors with super hybrid immunity

Human samples from individuals with SH, of both sexes, were collected through a collaboration with the Azienda Ospedaliera Universitaria Senese, Siena (IT). All subjects enrolled gave their written consent. The study that allowed the enrollment of subjects in all three cohorts was approved by the Comitato Etico di Area Vasta Sud Est (CEAVSE) ethics committees (Parere 17065 in Siena, amendment 13 December 2021) and conducted according to good clinical practice in accordance with the declaration of Helsinki (European Council 2001, US Code of Federal Regulations, ICH 1997). This study was unblinded and not randomized. Six subjects were enrolled in super hybrid immunity cohort. Subjects in the SH cohort were exposed two times to SARS-CoV-2 infection and received three or four mRNA vaccine doses. First infections occurred between October 2020 and July 2022, while second infections occurred between January and December 2022. Vaccinations occurred between December 2020 and December 2022. Given the exploratory nature of this study, no statistical methods were used to predetermine sample size. All super hybrid donors' clinical details are reported in Table S1.

Viral strains and cell culture

The SARS-CoV-2 viruses used to perform the CPE-MN neutralization assay were the Wuhan (SARS-CoV-2/INMI1-Isolate/2020/Italy: MT066156), Omicron BA.5 (GISAID ID: EPI_ISL_13389618), BA.2.75 (GISAID ID: EPI_ISL_14732896), BF.7 (GISAID ID: EPI_ISL_13499917), BQ.1.1 (GISAID ID: EPI_ISL_15455664), XBB.1.5 (GISAID ID: EPI_ISL_17272995), EG.5.1.1 (GISAID ID: EPI_ISL_18245523) and BA.2.86 (GISAID ID: EPI_ISL_18221650). The BA.2.86 strain (hCoV-19/France/IDF-IPP17625/2023) was supplied by the National Reference Center for Respiratory Viruses hosted by Institut Pasteur (Paris, France). The human sample from which strain hCoV-19/France/IDF-IPP17625/2023 was isolated has been provided by Dr Aude LESENNE from Cerballiance Ile De France Sud, Lisses. 3T3-msCD40L Cells were used as feeder cells for single cell sorting (NIH AIDS Reagent Program, Cat#12535). VERO E6 cell (ATCC, Cat#CRL-1586) were used to perform SARS-CoV-2 live virus neutralization assays. Small and large scale expression of monoclonal antibodies was performed in Expi293F cells (Gibco, Cat#A14527). Human coronaviruses S proteins were expressed using ExpiCHO-S Cells (Gibco, Cat# A29127). HEK293TN-hACE2 (System Bioscience, Cat#LV900A-1), HUH7 (Japanese Collection of Research Bioresources (JCRB), JCRB-0403), CHO-K1 (ATCC, CCL-61) and HEKTN/17 (ATCC, CRL-11268) cell lines were used for pseudovirus neutralization assays. THP-1 (ATCC, Cat#IB-202) were used to evaluate antibody ADCP.

METHOD DETAILS

Single cell sorting of SARS-CoV-1 and SARS-CoV-2 S-protein$^+$ memory B cells from COVID-19 vaccinees

Peripheral blood mononuclear cells (PBMCs) isolation was performed as previously described.[6,7,26] Briefly, PBMCs were isolated from heparin-treated whole blood by density gradient centrifugation (Ficoll-Paque PREMIUM, SigmaAldrich). After separation, cells were incubated at room temperature for 20 min with the viability dye Live/Dead Fixable Aqua (Invitrogen; Thermo Scientific). Then, cells were washed with PBS and incubated with 50 μL of 20% normal rabbit serum (Life technologies) diluted in PBS to saturate unspecific bindings. After 30 min of incubation at 4°C, cells were washed with PBS and stained with SARS-CoV-1 S-protein labeled with Strep-TactinXT DY-649 (iba-lifesciences cat# 2-1568-050) and SARS-CoV-2 S-protein labeled with Strep-TactinXT DY-488 (iba-lifesciences cat# 2-1562-050) for 30 min at 4°C. Then, a surface staining was performed using CD19 V421 (BD cat# 562440), IgM PerCP-Cy5.5 (BD cat# 561285), CD27 PE (BD cat# 340425), IgD-A700 (BD cat# 561302), CD3 PE-Cy7 (BioLegend cat# 300420), CD14 PE-Cy7 (BioLegend cat# 301814), CD56 PECy7 (BioLegend cat# 318318). After 30 min of incubation at 4°C, stained memory B cells were single cell-sorted with BD FACSAria Fusion (BD Biosciences), for donors SH-VAC-004, -009, −011, −012, and BD FACS Aria III (BD Biosciences) for donors SH-VAC-013 and -014, into 384-well plates and were incubated for 14 days with IL-2, IL-21 and irradiated 3T3-CD40L as previously described.[54]

SARS-CoV-2 authentic viruses neutralization assay

All SARS-CoV-2 authentic virus neutralization assays were performed in the biosafety level 3 (BSL3) laboratories at Toscana Life Sciences in Siena (Italy), which is approved by a Certified Biosafety Professional and inspected annually by local authorities. To assess the neutralization potency and breadth of nAbs against live SARS-CoV-2 and its variants, a cytopathic effect-based microneutralization assay (CPE-MN) was performed as previously described.[6,7,13,26] Briefly, 100 median Tissue Culture Infectious Dose (100 $TCID_{50}$) of SARS-CoV-2 virus was co-incubated with nAbs for 1 h at 37°C, 5% CO_2. The virus-antibody mixtures were then moved into a 96-well plate containing a sub-confluent Vero E6 cell monolayer. Plates were incubated for 3–4 days at 37°C in a humidified environment with 5% CO_2, then examined for CPE by means of an inverted optical microscope by two independent operators. Single cell sorting supernatants were tested at single point dilution to identify positive hits and antibody to be recombinantly expressed through transcriptionally active polymerase chain reaction (TAP-PCR). TAP supernatant, used to evaluate the neutralization potency of identified nAbs, were tested at a starting dilution of 1:4 and diluted step 1:2. Single replicate and technical duplicates were performed to evaluate single cell sorting supernatant and to evaluate the IC_{100} of TAP respectively. In each plate positive and negative control were used as previously described.[6,7,13,26]

Single cell RT-PCR and Ig gene amplification and transcriptionally active PCR expression

To express our nAbs as full-length IgG1, 5 μL of cell lysate from the original 384-cell sorting plate were used for reverse transcription polymerase chain reaction (RT-PCR), and two rounds of PCRs (PCRI and PCRII-nested) as previously described.[6,7,26] Obtained PCRII products were used to recover the antibody heavy and light chain sequences, through Sanger sequencing, and for antibody cloning into expression vectors as previously described.[6,7,26] TAP-PCR reaction was performed using 5 μL of Q5 polymerase (NEB), 5 μL of GC Enhancer (NEB), 5 μL of 5X buffer,10 mM dNTPs, 0.125 μL of forward/reverse primers and 3 μL of ligation product, using the following cycles: 98°/2′, 35 cycles 98°/10″, 61°/20″, 72°/1′ and 72°/5'. TAP products were purified under the same PCRII conditions, quantified by Qubit Fluorometric Quantitation assay (Invitrogen) and used for transient transfection in Expi293F cell line following manufacturing instructions.

Expression and purification XBB.1.5, BA.2.86 and H-CoV S proteins

The plasmids encoding SARS-CoV-2 6P WT and for the seven S proteins of the season H-CoV was generously provided by Prof. Jason S. McLellan. All proteins were expressed and purified as previously described.[6] Briefly, plasmids encoding for XBB.1.5, BA.2.86 and H-CoV S proteins were transiently transfected in ExpiCHO-S cells (Thermo Fisher) using ExpiFectamine CHO Reagent. Cells were grown for six days at 37°C with 8% CO_2 in shaking conditions at 125 rpm according to the manufacturer's protocol (Thermo Fisher). ExpiFectamine CHO Enhancer and ExpiCHO Feed were added 18 to 22 h post-transfection to boost transfection, cell viability, and protein expression. Both types of cell cultures (for the spike of SARS-CoV-2 and H-CoVs) were harvested five days after transfection and the proteins were purified by immobilized metal affinity chromatography (FF Crude) followed by dialysis into final buffer. Cell culture supernatants were clarified by centrifugation (1,200x g, 30 min, 4°C) followed by filtration through a 0.45 μm filter. Chromatography purification was conducted at room temperature using ÄKTA Go purifier system from GE Healthcare Life Sciences. Specifically, filtered culture supernatant was purified with a 5 mL HisTrap FF Crude column (GE Healthcare Life Sciences) previously equilibrated in Buffer A (20 mM NaH2PO4, 500 mM NaCl +30 mM Imidazole pH 7.4). The flow rate for all steps of the HisTrap FF Crude column purification was 5 mL/min. The culture supernatant of each spike protein was applied to a single 5 mL HisTrap FF Crude column. The column was washed in Buffer A with 4 column volumes (CV). spike proteins were eluted from the column by applying a first step elution of 5CV of 60% Buffer B (20 mM NaH_2PO_4, 500 mM NaCl +500 mM Imidazole pH 7.4). Elution fractions were collected in 1 mL each and analyzed by SDS-PAGE. Fractions containing the S protein were pooled and dialyzed against PBS buffer pH 7.4 using Slide-A-Lyzer Dialysis Cassette 10K MWCO (Thermo Scientific) overnight at 4°C. The dialysis buffer used was at least 200 times the volume of the sample. The final spike protein concentration was determined by measuring absorbance at 562 nm using Pierce BCA Protein Assay Kit (Thermo Scientific). Proteins were dispensed into 0.5 mL aliquots and stored at −80°C.

ELISA assay with SARS-CoV-2 NTD, RBD and S2 subunits

To determine the binding specificity of nAbs to the SARS-CoV-2 S protein domains we performed and ELISA to the RBD, NTD and S2 domains. The assay was performed as previously described.[7,26] Briefly, 3 μg mL^{-1} of SARS-CoV-2 subunits diluted in carbonate-bicarbonate buffer (E107, Bethyl Laboratories), were coated in 384-well plates (microplate clear, Greiner Bio-one), and blocked with 50μL/well of blocking buffer (phosphate-buffered saline, 1% BSA) for 1h at 37°C. After washing (phosphate-buffered saline and 0.05% Tween 20), plates were incubated with mAbs diluted 1:5 in dilution buffer (phosphate-buffered saline, 1% BSA, 0.05% Tween 20) and step-diluted 1:2 in dilution buffer. Anti-Human IgG-Peroxidase antibody (Fab specific) produced in goat (Sigma) diluted 1:45,000 in dilution buffer for RBD and NTD plates, while 1:80,000 in dilution buffer for S2 plates, was added and incubated for 1h at 37°C. Plates were then washed, incubated whit TMB substrate (Sigma) for 15 min before adding 25 μL/well of stopping solution (H_2SO4 0.2M). The OD values were identified using the Varioskan Lux Reader (Thermo Fisher Scientific) at 450 nm. Each condition was tested in duplicate and samples were considered positive if the OD value was 2-fold the blank.

ELISA assay with H-CoVs S proteins

Antibody binding specificity against the H-CoVs SARS-CoV-1, 229E, OC43 and HKU-1 S proteins was detected by ELISA as previously described.[13] Briefly, 384-well plates (microplate clear, Greiner Bio-one) were coated with 3 μg mL^{-1} of streptavidin (Thermo Fisher) diluted in carbonate-bicarbonate buffer (E107, Bethyl Laboratories) and incubated at RT overnight. The next day, plates were incubated for 1h at RT with 3 μg mL^{-1} of H-CoVs S proteins, and saturated with 50 μL/well of blocking buffer (phosphate-buffered saline, 1% BSA) for 1h at 37°C. Following, 25 μL/well of mAbs diluted 1:5 in dilution buffer (phosphate-buffered saline, 1% BSA, 0.05% Tween 20) were added and serially diluted 1:2 and then incubated for 1h at 37°C. Finally, 25 μL/well of alkaline phosphatase-conjugated goat Anti-Human IgG diluted 1:2,000 in dilution buffer were added. mAbs binding to the S proteins were detected using 25 μL/well of PNPP (*p*-nitrophenyl phosphate; Thermo Fisher) and the reaction was measured at a wavelength of 405nm using the Varioskan Lux Reader (Thermo Fisher Scientific). After each incubation step, plates were washed with washing buffer (phosphate-buffered saline and 0.05% Tween 20). Sample buffer was used as a blank and the threshold for sample positivity was set at 2-fold the OD of the blank. Technical duplicates were performed.

SARS-CoV-1 pseudotype based microneutralization assay

To screen single cell sorting supernatants and identify mAbs able to neutralize SARS-CoV-1 we performed a microneutralization assay in 384 well-plates. The HEK293TN-hACE2 cell line was generated by lentiviral transduction of HEK293TN (System Bioscience, Cat#LV900A-1) cells as described in Notarbartolo S. et al.[55] SARS-CoV-1 lentiviral pseudotype particles were generated as described in Conforti et al. using the SARS-CoV1 SPIKE plasmid pcDNA3.3_CoV1_D28 (Addgene plasmid # 170447).[56] HEK293TN-hACE2 were plated 10,000/well in 384-well flat plates (Corning cat#3765) using DMEM medium complete (10% FBS, 2mM L-glutamine, 1% Pen-strep,1mM Sodium pyruvate, 1% Non-Essential Amino Acid). After 24h, cells were infected with 0.1 MOI of SARS-CoV-1 pseudotyped viruses that were previously incubated with 7 μL of each mAb supernatant. Supernatants were diluted 1:5 with a pseudotyped viral solution at 0.1 multiplicity of infection (MOI) and were tested at single point dilution. PBS and the mAb S309 (tested starting from 10 μg mL^{-1} and serially diluted step 1:3) were used as negative and positive controls respectively. The mix was incubated for 1h at 37°C and then 25 μL were added into 50 μL of HEK293TN-hACE2 pre-seeded wells. Plates were incubated at 37°C for 24h after which luciferase activity was measured reading the plate on Varioskan LUX (Thermo Scientific) using the Bright-Glo Luciferase Assay System (Promega), according to the manufacturer's recommendations. Percent of inhibition was calculated relative to pseudotype virus-only control. 50% neutralization dose (ND_{50}) values were established by nonlinear regression using Prism v.8.1.0 (GraphPad).

H-CoV (229E, HKU-1 and OC43) pseudotype based microneutralization assays

The neutralization assay for 229E, HKU-1 and OC43 H-CoV pseudotyped viruses was performed as described for SARS-CoV-1 pseudotype virus using 96-well plates. In addition, appropriate cell lines expressing H-CoVs receptor were used to allow infection and evaluation of neutralization activity of isolated nAbs. Specifically, HUH7, CHO-K1 and HEKTN/17 cell lines were used for 229E, HKU-1 and OC43 respectively. Briefly, 100 μL containing $1x10^4$ cells were plated in each well in white 96-well plates using DMEM medium complete (10% FBS, 2mM L-glutamine, 1% Pen-strep,1mM Sodium pyruvate, 1% Non-Essential Amino Acid). 24h later, cells were infected with 0.1 MOI of pseudotyped viruses that were previously co-incubated for 1h at 37°C with serial dilution of TAP supernatants in 50 μL. A 7-point dose-response curve was obtained by diluting TAP supernatants step 1:3. After 24 incubation at 37°C for 24h, luciferase activity was measured reading the plate on Varioskan LUX (Thermo Scientific) using the Bright-Glo Luciferase Assay System (Promega), according to the manufacturer's recommendations. Percent inhibition was calculated relative to pseudotype virus-only control. ND_{50} (Neutralization Dose) values were established by nonlinear regression using Prism v.8.1.0 (GraphPad). The average ND_{50} value for each antibody was determined from a minimum of three independent technical replicates and two independent experiments. Technical triplicates were performed.

Flow cytometry-based competition assay

To characterize mAb candidates based on their interaction with S protein epitopes, a flow cytometry-based competition assay was performed. As previously described,[7] 1 mg of magnetic beads (Dynabeads His-Tag, Invitrogen) were coupled with 200 μg of histidine-tagged SARS-CoV-2 S protein. Then, S protein-beads (20 μg mL^{-1}) were incubated with unlabeled neutralizing antibodies at room temperature for 40 min and the sample was subsequently washed in PBS-1% BSA. To evaluate the S protein epitope competition, antibodies RBD Class 1/2 (J08), Class 3 (S309), Class 4 (CR3022) binders or NTD (4A8) binders were labeled with different fluorophores (Alexa Fluor 647, 488, 594) using the Alexa Fluor NHS Ester kit (Thermo Scientific). Next, fluorescent labeled antibodies were incubated with S protein-beads for 40 min at RT. After incubation, the S protein-antibodies mix was washed with PBS, resuspended in 150 μL of PBS-BSA 1%, and analyzed using BD FACSymphony A3 (BD Biosciences). As positive and negative controls, beads with or without S protein incubated with labeled antibodies were used. FACSDiva Software (version 9) and FlowJo (version 10) were used for data acquisition and analysis, respectively.

Measurement of ADCP and ADCD functions triggered by neutralizing antibodies

Antibody-dependent cellular phagocytosis (ADCP) was performed using a Flow cytometry–based assay. As previously described,[57] stabilized histidine-tagged SARS-CoV-2 S protein (Wuhan, XBB.1.5, BA.2.86) was labeled with Strep-TactinXT Conjugate DY- 649 (IBA Lifesciences) and conjugated to magnetic beads according to the manufacturer's instructions. The mix S protein-beads was incubated with nAbs for 1 h at RT and then mixed with monocytic THP- 1 cell line (50.000 per well). After 18h of incubation at 37°C, THP-1 cells were washed with PBS and fixed with fixation buffer (BioLegend) following the manufacturer's guidelines. Next, cells resuspended in 100 μL of PBS1X were acquired by BD FACSymphony A3 (BD Biosciences). FlowJo software (version 10) was used for data analysis and phagocytosis was evaluated as percentage of fluorescent beads engulfed by THP-1 multiplied by the median fluorescence intensity of the population. To explore the antibody dependent complement deposition (ADCD), Expi293F cells (Thermo Fisher, Cat#A14527) were transiently transfected with SARS-CoV-2 original S protein, XBB.1.5, or BA.2.86 expression vectors (pcDNA3.1_ spike_del19) using the ExpiFectamine Enhancer (Thermo Fisher).[57] After 48h, monoclonal antibodies were incubated with S protein-expressing cells at 37°C, with 5% CO_2 and 120 rpm shaker speed for 30 min. Then, 6% of baby rabbit complement (Cedarlane) diluted in Expi medium was added, and cells were incubated at 37°C, with 5% CO_2 and 120 rpm shaker speed. After 30 min of incubation, cells were incubated with goat anti-rabbit polyclonal antibody against C3-FITC conjugated (MP Biomedicals) for 1 h on ice. Then, stained cells were fixed with fixation buffer (BioLegend) for 15 min on ice and resuspended in 100 μL of PBS. BD FACSymphony A3 (BD Biosciences) was used for data acquisition and results were reported as median fluorescence intensity of

the FITC signal detected. Potencies for ADCP and ADCD were reported as previously described.[57] For ADCP, an unrelated plasma was used as negative control and the threshold for sample positivity was set at 3-fold the ADCP score of the negative control. Based on this cut-off point, nAbs were classified as high (>8-fold the threshold), medium (>4-fold the threshold), or low (up to 4-fold the threshold) phagocytosis inducers and given the extent of our nAb panel, antibodies were tested at a single-point dilution. As for ADCD, based on the mean fluorescent intensity (MFI) value of the negative control, nAbs were classified as high (>8-fold the threshold), medium (>4-fold the threshold), or low (up to 4-fold the threshold) ADCD inducers. Radar plots were generated to report the ADCP, ADCD and neutralization activities of all RBD classes and NTD binding nAbs against SARS-CoV-2 Wuhan, XBB.1.5 and BA.2.86. The results are presented as percentage of positive nAbs in the functional assay (ADCP, ADCD, or neutralization). The analysis was performed using Pandas v1.3.5 and the radar plots were created using Matplotlib v3.2.2 in Python.

Functional repertoire analyses

nAbs VH and VL sequence reads were manually curated and retrieved using CLC sequence viewer (Qiagen). Aberrant sequences were removed from the dataset. Analyzed reads were saved in FASTA format and the repertoire analyses was performed using Cloanalyst (http://www.bu.edu/computationalimmunology/research/software/).[58,59]

Network plot of clonally expanded antibody families

A network map was built by representing each clonal family with a centroid and connecting centroids sharing a similar sequence. The centroid sequence was computed with Cloanalyst to represent the average CDRH3 sequence for each clonal family, and Hamming distance was calculated for each antibody CDRH3 sequence to represent the relationship within the clonal family. Levenshtein distance was calculated between each centroid representative of each clonal family to investigate the relationship between clonal families. Levenshtein distance was calculated with the R package stringdistm v0.9.8 (https://cran.r-project.org/web/packages/stringdist/index.html) and normalized between 0 and 1. Centroids showing at least 80% of CDRH3 sequence similarity were connected. A network graph was generated with the R package ggraph v2.0.5 (https://ggraph.data-imaginist.com/index.html) with Fruchterman-Reingold layout algorithm and the figure was assembled with ggplot2 v3.3.5. The size of the centroid is proportional to the number of antibodies belonging to the same clonal family, while the color of each node represents the antibody origin: pink for seropositive 2nd dose (SP2), and dark red for superhybrids (SH).

Alluvial plot of germline frequency distribution

An alluvial plot was generated to display the frequency distribution of IGHV; IGHJ germ lines among the two analyzed cohorts: seronegative 3rd dose (SN3) and superhybrids (SH). The cohorts are represented as two separate categories (strata), and the germline frequency for each single cohort is represented by the flow size. The analysis included all antibodies with fully sequenced VH chains, totaling 289 entries for SN3 and 441 entries for SH. The change in IGHV; IGHJ germline frequency amoung the two cohorts was evaluated, and the five germ lines with higher, unaltered frequency were highlighted. Specifically, germline IGHV3−66; IGHJ6, IGHV3−53; IGHJ6, IGHV1−69; IGHJ4, IGHV1−69; IGHJ3, and IGHV1−58; IGHJ3 were selected. Additionally, germ lines not observed in the SN3 cohort but comprising more than five entries in the SH cohort (IGHV5−10−1; IGHJ4, IGHV3−21; IGHJ6, IGHV1−2; IGHJ4, IGHV1−24; IGHJ4, IGHV1−18; IGHJ4) were highlighted within the SH stratum using a black rectangle. Spider plots were created for each cohort to depict the functionality of the selected germ lines in terms of neutralization, antibody-dependent cellular phagocytosis (ADCP), and antibody-dependent complement deposition (ADCD). The percentage of functional antibodies associated with each germ line was determined using predefined thresholds of 100,000, 100,000, and 4,000 for neutralization, ADCP, and ADCD, respectively. The figure was assembled with ggplot2 v3.3.5. All the scripts and the data are available via github (https://github.com/dasch-lab/SARS-CoV-2_superhybrid).

QUANTIFICATION AND STATISTICAL ANALYSIS

Statistical analysis was assessed with GraphPad Prism Version 8.0.2 (GraphPad Software, Inc., San Diego, CA). Nonparametric Mann-Whitney t test was used to evaluate statistical significance between the two groups analyzed in this study. Statistical significance was shown as * for values $\leq$0.05, ** for values $\leq$0.01, and *** for values $\leq$0.001.